Glacial Vermicular Ridge Features on Axel Heiberg Island, Nunavut, Canada

Shannon M. Hibbard[1,2], Gordon R. Osinski[3], Etienne Godin[4], Chimira Andres[5], Antero Kukko[6,7], Shawn Chartrand[8], Anna Grau Galofre[9], A. Mark Jellinek[10], Wendy Boucher[11]

[1]Division of Earth and Ecosystem Sciences, Desert Research Institute, Reno, Nevada, 89512, USA
[2]Jet Propulsion Laboratory, California Institute of Technology, Pasadena, California, 91101, USA
[3]Department of Earth Sciences, University of Western Ontario, London, Ontario, N6A 5B7, Canada
[4]Centre d'Études Nordiques, Université Laval, Québec, Québec, Canada, G1V 0A6
[5]Lassonde School of Engineering, York University, Toronto, Ontario, M3J 1P3, Canada
[6]UNITE Flagship, Department of Remote Sensing and Photogrammetry, Finnish Geospatial Research Institute, Espoo, Finland
[7]Department of Built environment, Aalto University, Espoo, Finland
[8]School of Environmental Science, Simon Fraser University, Burnaby, British Columbia, V5A 1S6, Canada
[9]Laboratoire de Planétologie et Géosciences, CNRS UMR 6112, Nantes, France
[10]Department of Earth, Ocean and Atmospheric Sciences, University of British Columbia, V6T 1Z4, Canada
[11]Department School of Graduate Studies, Trent University, Peterborough, Ontario, K9L 0G2, Canada

Correspondence to: Shannon M. Hibbard (shannon.hibbard@dri.edu)

Abstract. Vermicular Ridge Features (VRFs) consist of a series of ridges and troughs with a circular, sinuous, and anastomosing morphology. This newly recognized Arctic landform was initially identified on the south coast of Devon Island, Nunavut, Canada. Here, we report on the identification of VRFs near Mokka Fjord on Axel Heiberg Island, Nunavut, Canada. Utilizing field observations, ultra-high resolution LiDAR, and ground penetrating radar, we characterize and compare the morphometry and sedimentology of VRFs at Mokka Fjord with other periglacial, paraglacial, and glacial landforms. The VRFs near Mokka Fjord range in diameter from 6 to 37 m and reach up to 1.5 m in height and are composed of clast-rich glaciofluvial sediment and till. We considered two possible formation mechanisms: a periglacial origin (i.e., segregation ice features/lithalsas) and glacial origin (i.e., ring-ridge moraines and kettled outwash/kame terraces). Although we do not rule out either proposed mechanism, our preferred interpretation is that the Mokka Fjord VRFs are an ice-marginal feature resulting from paraglacial ablation of buried glacial ice, leading to the formation of hummocky ring-ridges composed of ice-marginal glaciofluvial sediment and likely also supra- and englacial debris. This formation mechanism suggests a predominantly polythermal glacial environment with limited water supply throughout much of the Holocene.

1 Introduction

The Canadian high arctic and has been subject to glacial and periglacial processes throughout the Quaternary Period. These processes can produce a wide variety of landforms, many of which are/were associated with massive ice. These landforms can often appear morphologically very similar and, thus, be difficult to differentiate. This has led to ongoing debate within the fields of periglacial and glacial geomorphology. This is especially difficult in the Canadian high arctic (e.g., French and Harry, 1990) given how remote it is and considering that it has only recently undergone deglaciation and is, therefore, a predominantly paraglacial landscape that has experienced the effects of both recent glaciation and periglacial modification.

Much of the Canadian high arctic lies in an environment favorable to polythermal and cold-based glaciers, which limits the glacial imprint on a landscape. Therefore, evidence of glaciation might be expected in the form of buried snout/ice-marginal glacial ice susceptible to glacial karst development, hummocky till veneers, glaciofluvial outwash, and kames (O' Cofaigh et al., 2003). However, periglacial processes can lead to hummocky terrain in till and glaciofluvial outwash sediments and produce buried massive ice through ice segregation and injection (French and Harry, 1990), which can become susceptible to thermokarst degradation. The topographic inversion of glacial sediments (e.g., Fairbridge, 1968; Thompson et al., 2016; Westoby et al., 2020) due to the ablation of underlying glacial ice is a common mechanism for the production of hummocky surfaces in deglaciated landscapes (e.g., Clayton, 1964; McKenzie, 1969; Embleton and King, 1975; Knudsen et al., 2006; Krüger et al., 2010; Moore, 2021). This process usually forms a series of landforms characterized by mounds and depressions following the retreat of a glacier and has been observed to create conspicuous circular (e.g., Gravenor and Kupsch, 1959) to sinuous and anastomosing (e.g., Knudsen et al., 2006; Hibbard et al., 2021) morainic ridges. Yet, the ablation of buried non-glacial ice can produce morphologically similar features (e.g., Mackay, 1974; Rampton, 1988; Mollard, 2000), the origin of which is still be a topic of debate (e.g., Watson and Watson, 1974; Ross et al., 2019).

While these features may appear similar in the field, the processes by which they formed are very different. Both massive buried glacial ice and segregation ice are common across the Canadian high arctic (O'Neill et al., 2019). Differentiating between massive ice origins and the associated landform origins are key to understanding the evolution of high arctic landscapes and reconstructing Quaternary environmental conditions. This is especially true in continuous permafrost zones, where the presence of massive segregation ice and periglacial landforms can inform us about climate during deglaciation and affects climate change has in high arctic environments.

We report here on an undocumented landform on the east coast of Axel Heiberg Island near Mokka Fjord in Nunavut, Canada, that appears remarkably similar to Vermicular Ridge Features (VRFs) recently identified at Dundas Harbour on Tallurutit (Devon Island) (Hibbard et al., 2021). VRFs comprise a series of ridges and troughs with a circular, sinuous, to anastomosing, and therefore "worm-like," morphology. We refer to these features as Vermicular Ridge Features (VRFs) as a descriptive term without any genetic interpretation. We provide a comparison of Mokka Fjord VRF morphometrics, substrate characteristics, and associated landforms and processes, to other morphologically similar glacial and periglacial landforms and present a working hypothesis for the formation of this landform and the implications it has on past climate conditions during the Holocene.

2 Geologic and Geomorphic Setting

Axel Heiberg Island (Umingmat Nunaat) is located in the Qikiqtani region of Nunavut of Inuit Nunangat in Canada (Fig. 1). It is also part of the Sverdrup Islands in the Queen Elizabeth Islands of the Canadian Arctic Archipelago. Axel Heiberg Island lies within the thickest section (up to 13 km) of the Sverdrup Basin, which is predominantly composed of Carboniferous to Paleogene siliciclastics, evaporites, and carbonates (Balkwill, 1978; Russell et al., 2006; Embry and Beauchamp, 2008; Harrison and Jackson, 2014). Following the Pleistocene glaciations, Quaternary deposits (including stream, deltaic, glacial, and marine beach sediments) were deposited over bedrock geology and occupy valley floors and raised beach sediments along the coasts (Thorsteinsson, 1971a, 1971b).

The island hosts two major ice caps, the Müller Ice Cap and Steacie Ice Cap (Fig. 1a), and a wide range of glacier types such as cirque, outlet, piedmont, and valley glaciers (Ommanney, 1969; Thomson et al., 2011). The thermal regime of glaciers presently on Axel Heiberg Island are cold and polythermal (Blatter, 1987; Ó Cofaigh et al., 1999) which is thought to have extended into the last glacial maximum with the exception of fjord glaciers interpreted to be warm-based glaciers and ice streams (Ó Cofaigh et al., 1999; England et al., 2006). Axel Heiberg Island was covered by the Innuitian Ice Sheet, which reached its last glacial maximum around 29 ka BP (Bednarski, 1998). Extensive deglaciation of the Innuitian Ice Sheet occurred predominantly from west to east between 16.5 and 11 ka BP and marine-based ice largely disappeared by 9 ka BP leaving mostly land-based ice on Axel Heiberg and other islands (England et al., 2006). Deglaciation of the island proceeded and freed most of its fjords of ice by 8 ka BP (England et al., 2006) until reaching contemporary conditions around 7.5 ka BP. The marine limit varies across the Axel Heiberg Island but has been reported to range between 78 and 158 m asl (e.g., Bednarski, 1998; Pollard and Bell, 1998; Dyke et al., 2005).

Our field of study (Fig. 1b) lies within the Granite dispersal train (Ó Cofaigh et al., 2000; England et al., 2006) and is composed of Quaternary deposits (Thorsteinsson, 1971a, 1971b). Detailed surveying of VRFs was conducted at one main field site located on a terrace along a channel trending northwest-southeast feeding into Mokka Fiord. To our knowledge, this field site has not directly been analyzed for surficial geology and geomorphology in previous studies, but the coast of Nansen Sound and Flat Sound ~300 km to the northwest was surveyed by Bednarski (1998) who determined the area to be dominated by meltwater channels sourced from the western highlands, moraines and kame terraces, and marine sediments.

Present-day conditions represent a polar desert environment (Andersen et al., 2002). The nearest long-term climate station is Eureka A station located on the coast of Fosheim Peninsula on Mirnguiqsirvik (Ellesmere Island) ~ 300 km northeast of the field site. The Eureka A station reports a mean annual air temperature of −18.8°C and a mean annual precipitation of 79.1 mm (mostly in the form of snow—60.3 mm) between 1981 and 2010 (Environment Canada, 2021). Permafrost thickness has been measured to be 400 to 600 m at Mokka Fiord (Taylor and Judge, 1976; Pollard et al., 1999). Although the average climate equates to a polar desert, the Arctic is characterized by some of the most intense summertime climate variability resulting in wet precipitation and glacial/snow melting events (Constable et al., 2022) unlike a polar desert environment.

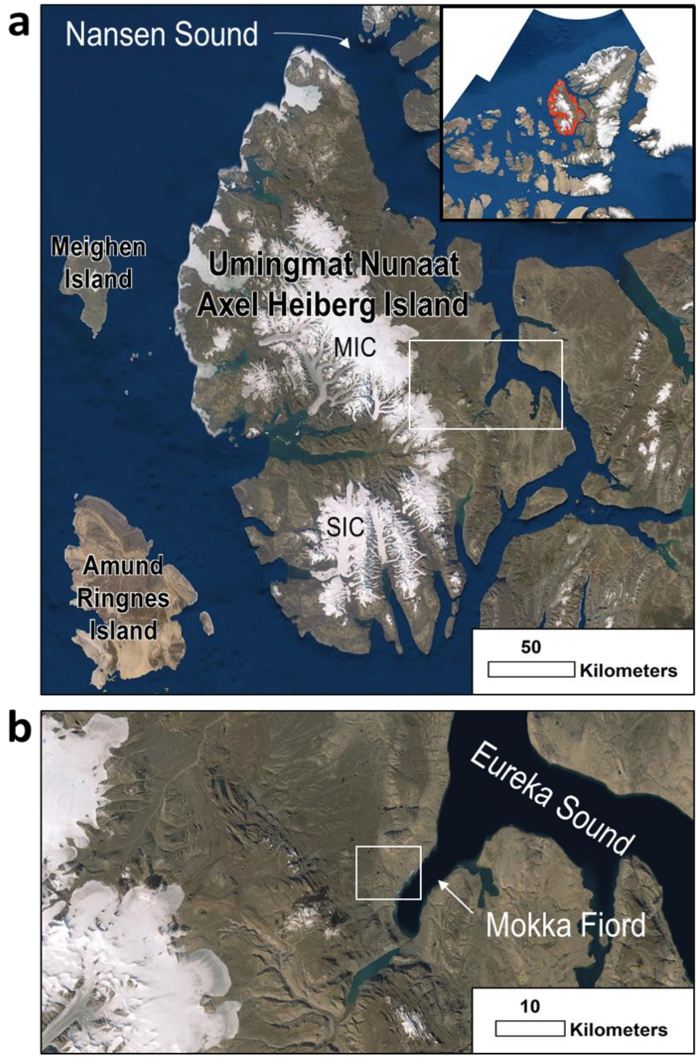

Figure 1: Axel Heiberg Island observed using World Imagery (Esri, 2018). (a) Axel Heiberg Island is located in Nunavut, Canada (outlined in red on top right). Nansen Sound runs along the east coast of much of Axel Heiberg Island. White box locates panel b. MIC and SIC represent Müller Ice Cap and Steacie Ice Cap, respectively. (b) Location of the field region (located within white box centered at 79.61589, -87.5556) is northeast of Mokka Fiord, which feeds into Eureka Sound. World Imagery Source: Esri, Maxar, GeoEye, Earthstar Geographics, CNES/Airbus DS, USDA, USGS, AeroGRID, IGN, and the GIS User Community.

3. Methodology

Fieldwork was carried out ~4 km northwest of Mokka Fiord on Axel Heiberg Island in July 2019 (Fig. 1). Field reconnaissance was done on foot and by helicopter which led to the identification of VRFs across multiple terraces along one river channel that feeds Mokka Fiord. A terrace along the channel was selected for in-depth field analysis, including trenching, Light Detection and Ranging (LiDAR), and Ground Penetrating Radar (GPR) data collection to characterize the landforms. AkhkaR4DW, a backpack mobile laser scanning system was used to kinematically collect high-precision 3D topographic data (Kukko et al., 2012; Liang et al., 2015; Kukko et al., 2017, 2020; Hyyppä et al., 2020). This system was developed by the Finnish Geospatial Research Institute to produce ultra-high resolution (1–5 cm-scale) digital elevation models (DEMs). The positioning of the system relies on post-processed tightly coupled differential processing of data from a GNSS receiver (NovAtel Pwrpak7) observing GPS and GLONASS satellite constellations and an inertial measurement unit (GNSS-IMU, NovAtel ISA-100C). For more details, see Kukko et al., (2020).

The LiDAR point cloud LAS file was produced using RiProcess and TerraScan software to filter and reduce the raw point cloud data which had a total of 46,163,219 points covering an area of ~6.42 ha with an average density of 164.2 points/m^2. WhiteBox Geospatial Analysis ToolBox (GAT), an open-source geospatial data analysis software developed by Professor John Lindsay at the University of Guelph (Lindsay, 2014, 2016), was used to create a Bare Earth DEM and Hillshade. The Bare Earth DEM was created using an inverse-distance weighting (IDW) scheme. A search distance of 10 cm was used to interpolate the point cloud. The Power (p) exponent was set to the default value of 2. Points that exceeded a slope of 30° from the unmeasured point being calculated were considered an outlier/non-ground point and were not used in the output point-cloud. A grid resolution of 5 cm/pixel was used to provide a high-resolution DEM with reasonably short processing time. The Hillshade azimuth (direction of the sun), measured clockwise from North, was set to 315° (northwest). The altitude (angle of illumination), measured from the horizon to normal, was set to 30°. The Bare Earth DEM and Hillshade files were loaded into ArcGIS Desktop 10.8.1 using a WGS 1984 UTM 16N projection.

A Sensors and Software 250 NOGGIN SmartTow GPR system was used to investigate massive ice and deposit thickness; the instrument was equipped with a 250 MHz antenna. Three GPR lines were collected, three of which lie within the LiDAR data, ranging from 20 to 30 meters in length. Signal velocity was determined based on sedimentology, diffraction hyperbola fitting, and context from trenching in the field, which was determined to be 0.125 m/ns (frozen and unfrozen sand and gravel). Based on this signal velocity, GPR signals penetrated down to roughly 4 m before heavily attenuating. GPR data was collected on July 8, 2019, therefore, the thaw depth is representative of that day of the year, which was measured/estimated at 1–1.5 m.

GPR data was analyzed using Sensors and Software’s Ekko_Project_5 software. GPR data was dewowed and was amplified with a Spherical Exponential Calibrated Compensation (SEC2) gain and an Attenuation value of 8. Elevation data along each GPR line was extracted from the LiDAR dataset and added to the GPR data file. This corrects for unreliable depths of key subsurface features, but slightly stretches the upper part of the cross-section image.

4 Observations and Results

4.1 Context and Setting of Mokka Fjord VRFs

We identified VRFs on seven terraces along a northwest-southeast trending meltwater channel flowing into Mokka Fiord (Figs. 2–4, and S1, Supp. files), five of which are located on the western side of the channel and two reside on the eastern side. The terraces occur at different elevations, with the uppermost terrace occurring at an average elevation of 166 m on the west side, and the lowermost terrace occurring at 114 m on the east side. An additional 5 VRF sites were identified up and down valley from the investigated terraces by helicopter (Figs. 2 and 3), one of which was located in the floodplain of the stream system (Fig. 3e). VRFs were also observed near Strand Fiord (Fig. 3g).

The VRFs at Mokka Fjord occur in three surficial geologic units mapped by the Geological Survey of Canada (2022), including (1) terraced sediments (At), comprised of coarse surface sediments and patterned ground, (2) till, morainal sediments, undifferentiated (T.W) comprised of marine reworked glacial diamicton, and (3) colluvial deposits, undifferentiated (C.W) comprised of a heterogeneous mixture of source rocks and grain sizes that are products of mass waste and have patterned ground. Our field observations support these regional interpretations and indicate that all VRFs occur in coarse-grained diamicton that is glacially or glaciofluvially sourced.

Polygonally patterned ground and solifluction were observed across the field sites. Ponds of water (Fig. 3e), wet soil (Figs. 3c, d), and thaw slumps (not seen in the 2011 Maxar image (Fig. 2) of the World Imagery data) (Fig. 4) were also observed at many of the VRF sites indicating active thermokarst degradation.

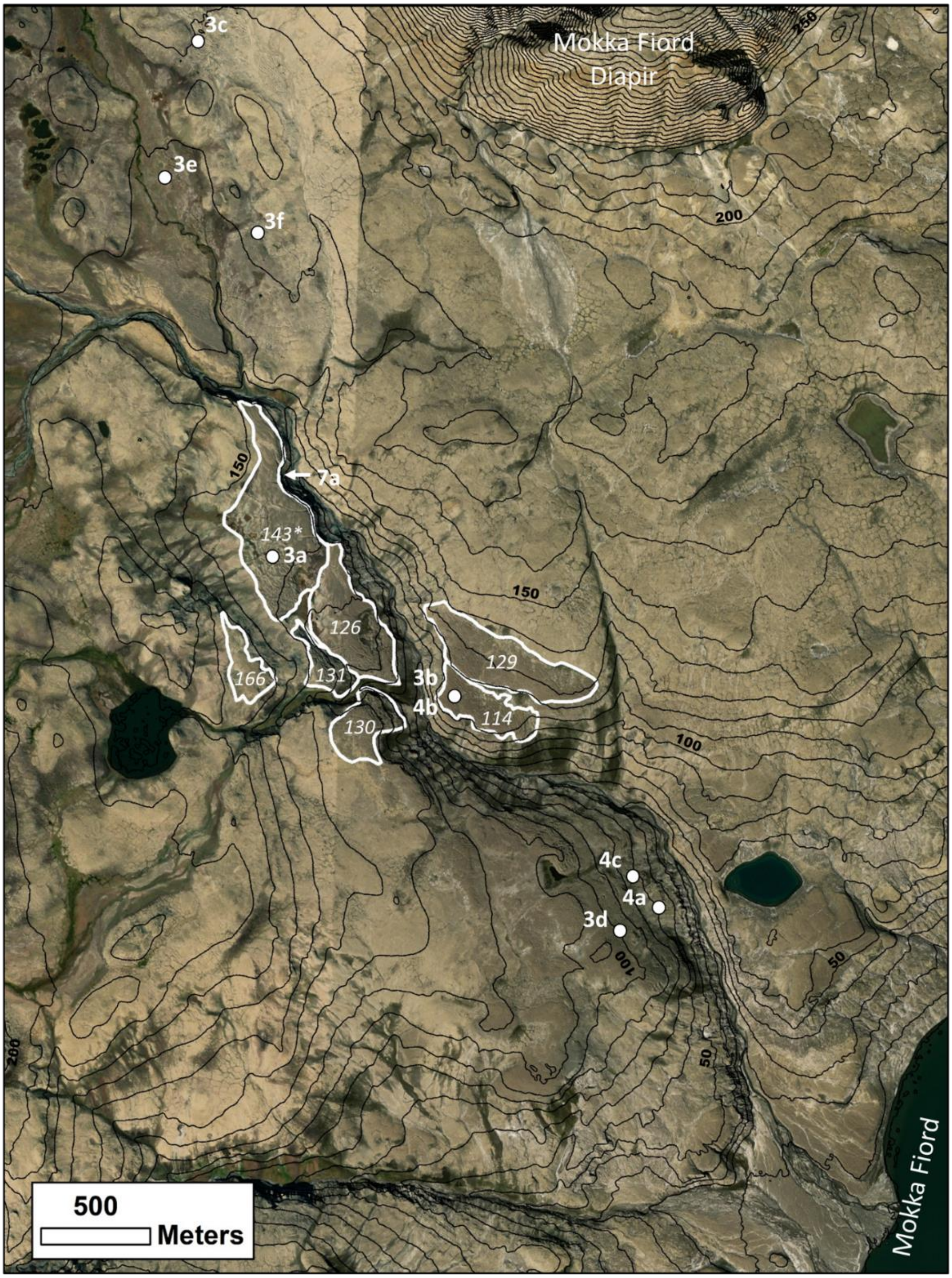

Figure 2: Maxar (WV02) image of the field region at Mokka Fiord in World Imagery taken in 2011 (Esri, 2018). Seven terraces containing VRFs are outlined in white. Average elevation (in meters) of each terrace is numbered in white. White dots indicate figure locations with figure numbers labelled in white. White arrow points to the location of the riverbank in Figure 7a. Elevation contours are labelled every 50 m and obtained from ArcticDEM Release 7 (Porter et al., 2018). The asterisked elevation denotes the main field site for in-depth field analysis (i.e., GPR, LiDAR, and trenching). World Imagery Source: Esri, Maxar, GeoEye, Earthstar Geographics, CNES/Airbus DS, USDA, USGS, AeroGRID, IGN, and the GIS User Community.

4.2 Morphologic Description of Mokka Fjord VRFs

VRFs found across the field region (Fig. 2) exhibit a circular, elongate, sinuous and/or anastomosing ridge and trough morphology in planform (Figs. 3 and 5). VRFs can create individual closed cells (i.e., ridges creating a closed loop encircling a central trough) that are circular (Figs. 3b, e, and 5), semi-circular (Figs. 3a, b, c, e, and 5) or elongated (Figs. 3c, f, and 5). VRFs range from being closely spaced and interconnected (Figs. 3a, b, d, g) to well-spaced and isolated (Fig. 3e), or somewhere in between (Figs. 3c, f, and 5). Minimal vegetation is found in the field region but can act as a distinguishing factor between the ridges and their surroundings (Figs. 3 and 5b).

One terrace was surveyed in detail (referred to as the main field site) to further investigate the VRFs (Figs. 2 and 5). VRFs at this site have raised convex ridges that stand above the rest of the deposit in which they reside and frequently encircle a central concave depression creating individual closed-cells (Fig. 5). Ridges can also be subdued, shallow and wide relative to the more prominent narrow convex ridges (Fig. 5). Small sharp-crested conical mounds (Fig. 3d) and rounded mounds (Fig. S1a,b, Supp. Files) can be found in the same deposit as VRFs. Terrain adjacent to the ridges and closed cells is referred to as the "mesh" which is the part of the deposit that interconnects VRFs (Fig. 6). The central depressions of closed-cell VRFs lie at the same elevation as or higher than the mesh with the ridges elevated above their adjacent terrain (Figs. 5 and 6). Topographic profiles (Fig. 6) of the VRFs show this mesh-ridge-trough sequence. The topographic lows (e.g., mesh and central depressions) at the main field site are poorly drained and host grasses and mosses (Fig. S1c, d, Supp. Files) compared to the dryer ridges that host lichens (Fig. S2, Supp. Files). A thin white salt crust can also be found across the VRF materials (i.e., the materials of which the ridges, troughs and mesh are composed) (Fig. 5a) generally found resting at the base of the ridges or in topographic lows.

The VRF materials at the main field site are cut by a stream exposing a ~6 m thick cliff that transitions into a ~12 m thick gentler sloping lobate material before connecting with the riverbed (Figs. 2 and 7a), suggesting the deposit has a minimum thickness of ~6 m at the river cutbank relative elevation. A pit was dug 89 cm into the mesh of the deposit without reaching the thaw depth (July 2019) (Fig. 7b). The deposit (observed at the cutbank and in the pit) is a gravelly diamicton composed of poorly sorted, clast-rich, sub-rounded to rounded silt, sand, pebbles and cobbles with minor evidence for a preferred flat orientation of large grains (Fig. 7b). Fewer cobbles were present below 70 cm in the pit. Small pits (~ 10 cm deep) were also dug in a ridge and central trough of a closed-cell VRF. No grain sorting was observed. A fabrics and grain size analysis were not done due to helicopter time constraints at the field site.

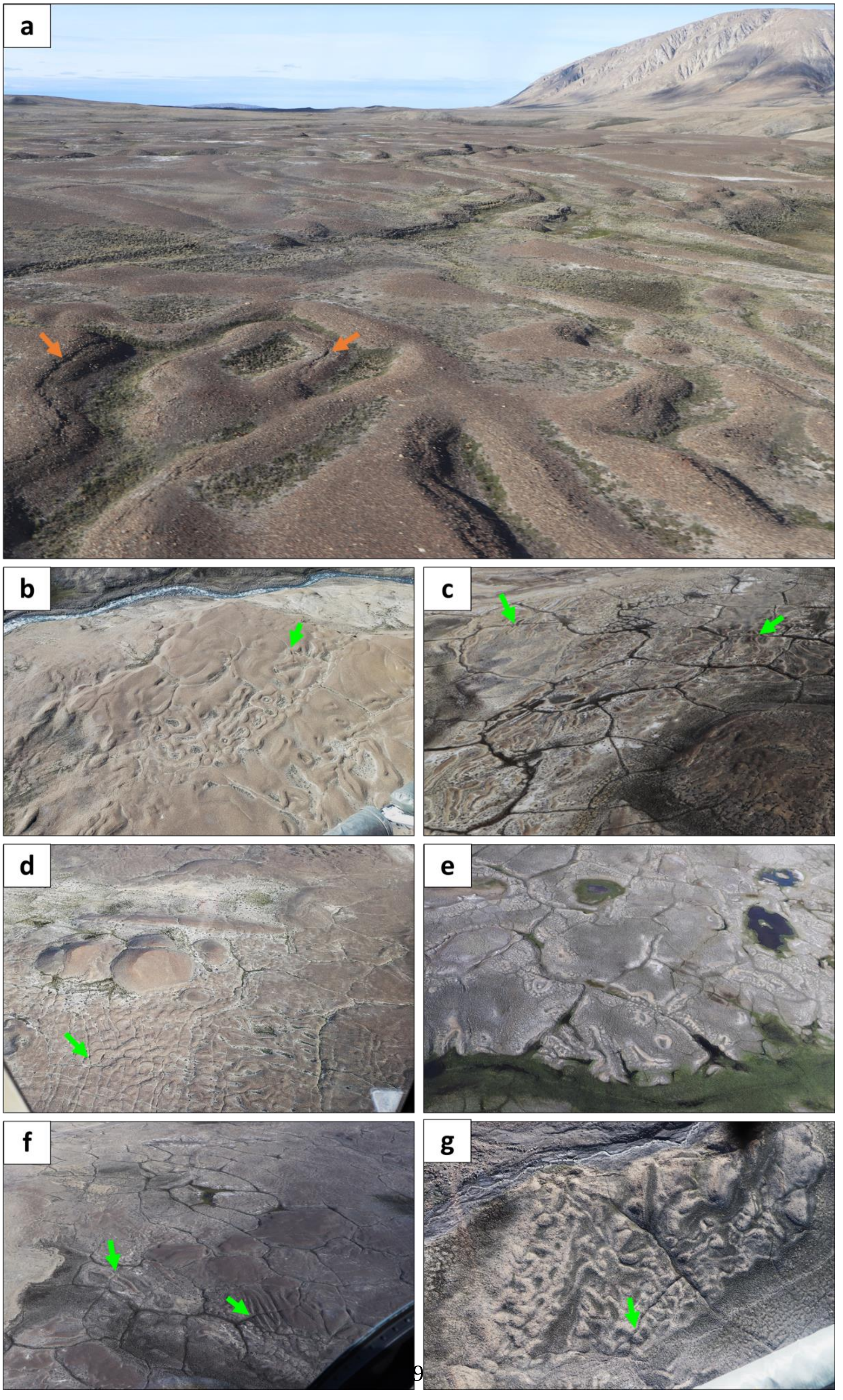

200

Figure 3: Examples of VRFs in the field as seen from a helicopter. Figure locations can be found in Figure 2. Green arrows show where VRFs are cross-cut by polygon troughs. (a) VRFs at the main field site near Mokka Fiord looking north. Mokka Fiord Diapir is in the background to the north. Cracks can be seen along or just off of the axial trace of some of the ridges (orange arrows). (b) VRFs on the terrace on the opposite side of the channel in the field region. (c) VRFs north of the field region, directly west of Mokka Fiord Diapir. (d) Sharp-crested mounds and VRFs south of the field site. (e) Light-toned VRFs north of the field region, west of Mokka Fiord Diapir. (f) Linear VRFs in a dark-toned deposit directly west of Mokka Fiord Diapir. (g) VRFs near Strand Fiord.

Ridges can reach up to 1.5 m in height when measured from the ridge apex to the adjacent low-lying terrain (i.e., mesh); although most do not exceed 1 m in height (Figs. 5 and 6). Closed-cell ridges (i.e., ridges that enclose a central depression) range in height between 0.2 and 0.6 m when measured from the lowest point in the central trough to the highest point on the ridge (Fig. 6). Ridge width ranges between 1.5 and 9 m but more commonly ranges between 3 and 4 m from the outer edges of the ridge (Fig. 5).

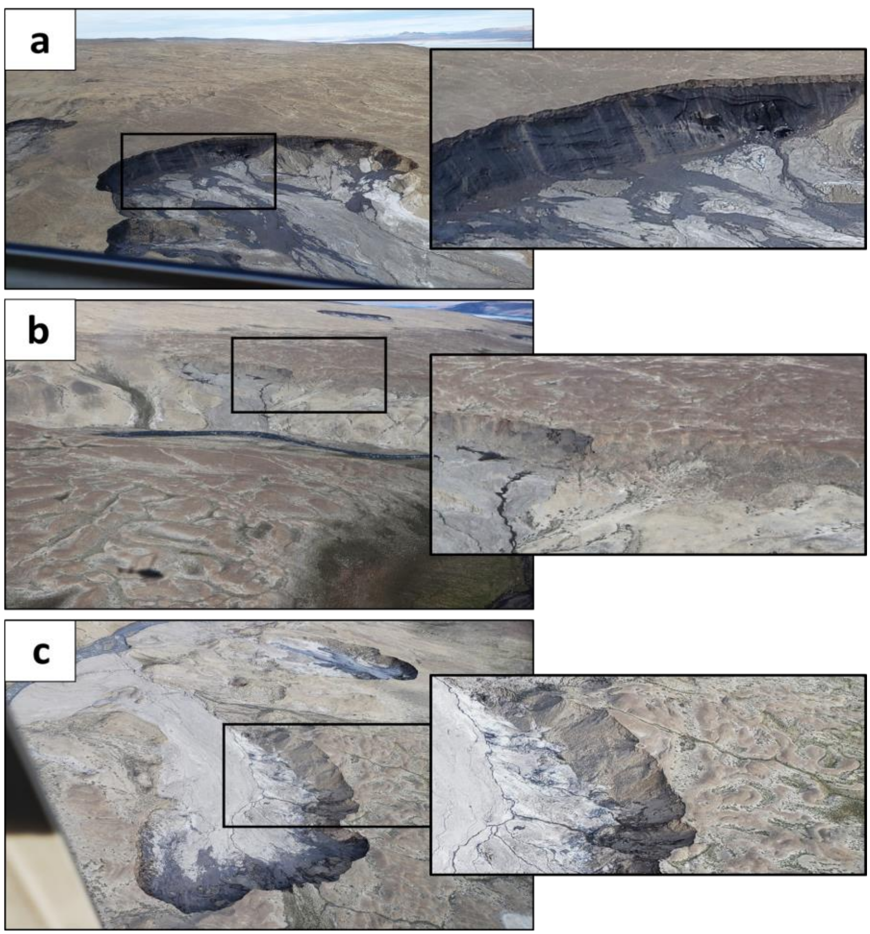

Figure 4: Thaw slumps in the field region. Figure locations can be found in Figure 2 by white dots. (a) West side of channel, south of field site. Possible massive ice exposed at thaw slump. Thaw slump exposure is around 10−15 m thick, including ~1−2 m of dry material above wet material. (b) East side of the channel, directly opposite the field site. A brown deposit with VRFs overlies a lighter-toned deposit. Overlying deposit thickness is around 10−15 m. (c) West side of channel, south of field site. Deposit with VRFs overlying lighter-toned sediments. Deposit thickness is roughly 10−15 m.

Thirty-two closed-cell VRFs with central troughs were mapped in the LiDAR area. The long axis of closed-cell ridges ranges between 5.8 and 36.8 m with an average of 15.8 m. The orientation of the long axes (north = 0°) range between 1.8° and 174.5° with an average of 95.7°. This orientation is near perpendicular to the roughly north-south running channel hosting the terraces (Fig. 2). The short axis of closed-cell ridges ranges between 4.3 and 12 m with an average of 8.2 m.

Cracks were found running along or just off-center from the axial trace of many ridges (Figs. 3a and S2, Supp. Files), and closed-cell ridges generally have a crack running off-center from the axial trace along the inner part of the cell (Fig. S2a, Supp. Files). Cracks present themselves as a thin and narrow cavity along the ridge (Figs. 6 and S2, Supp. Files), and slumping of the surrounding material may be present. Cracking also occurs along the center of polygon troughs and along the shoulders of polygons (Fig. S2c, Supp. Files), both of which tend to be much wider (≤ 30 cm) and deeper than the cracks observed on the ridges of VRFs.

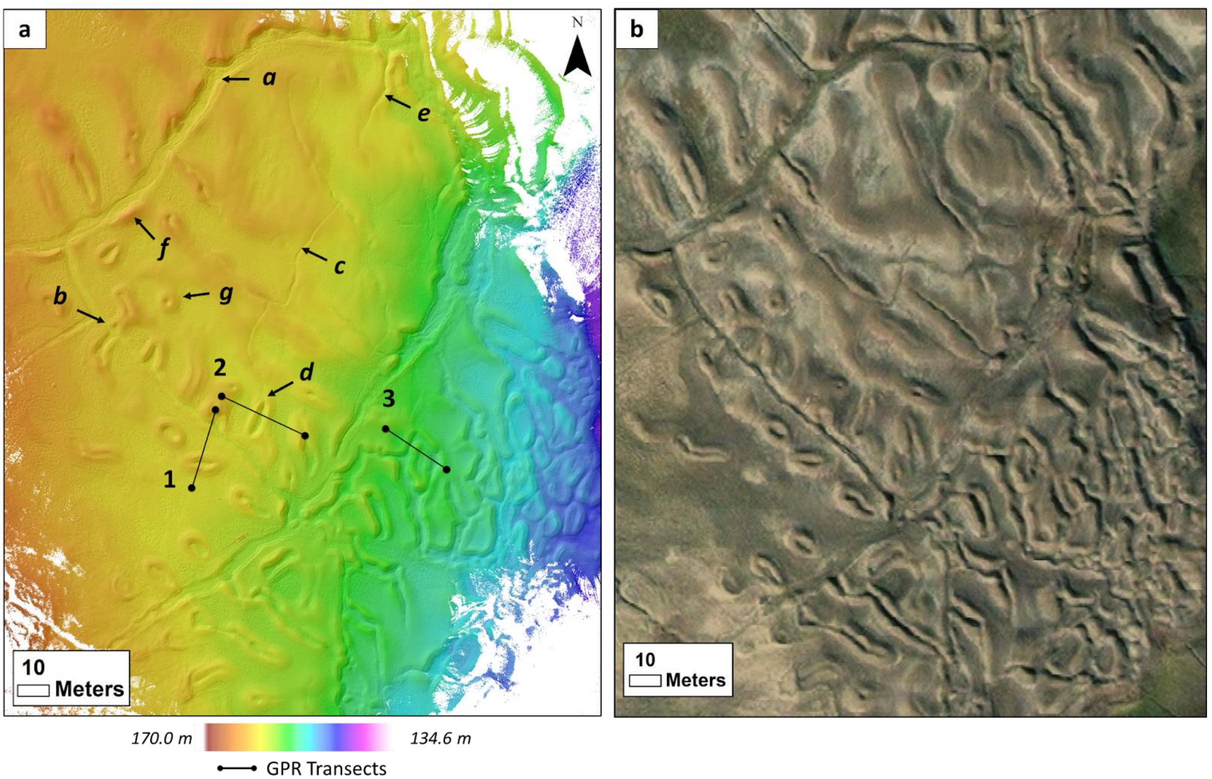

Figure 5: Digital Elevation Model of VRFs at the main field site. (a) DEM is overlying hillshade with 315° azimuth. GPR transects 1–3 are numbered and outlined in black. Topographic profiles and GPR transects can be found in Figure 6. Features of note include: a shallow and wide raised ridges cross-cut by polygon trough, b closed-cell VRF cross-cut by polygon trough, c secondary trough cross-cutting VRFs, d secondary trough cuts down through the middle of a closed-cell VRF, e secondary trough runs down the middle of a shallow sinuous VRF, f raised polygon shoulder, g perfectly circular individual closed-cell VRF. (b) Main field site LiDAR area in World Imagery (Esri, 2018). World Imagery Source: Esri, Maxar, GeoEye, Earthstar Geographics, CNES/Airbus DS, USDA, USGS, AeroGRID, IGN, and the GIS User Community.

a

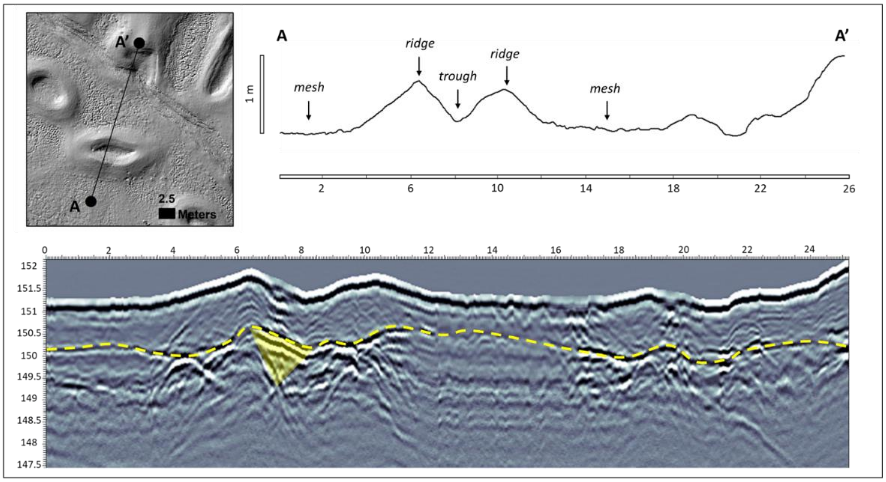
A
A'
2.5
Meters
mesh
ridge
trough
ridge
mesh
1 m

b

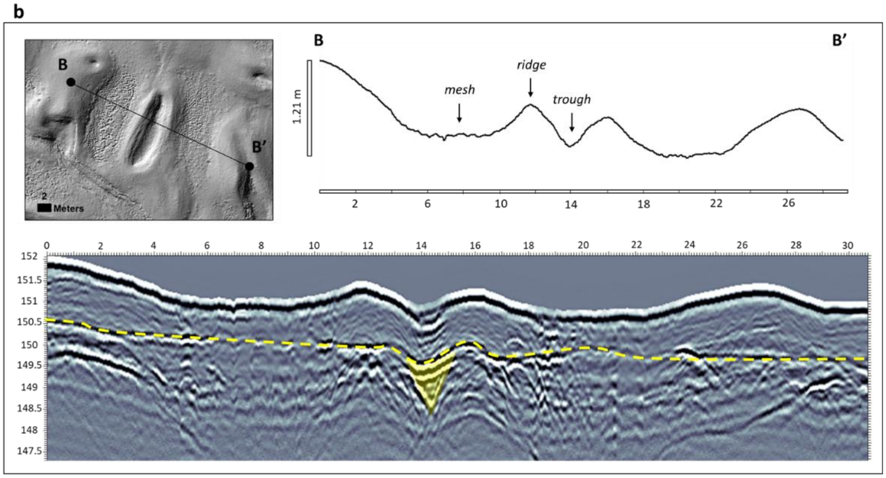
B
B'
2
Meters
mesh
ridge
trough
1.21 m

c

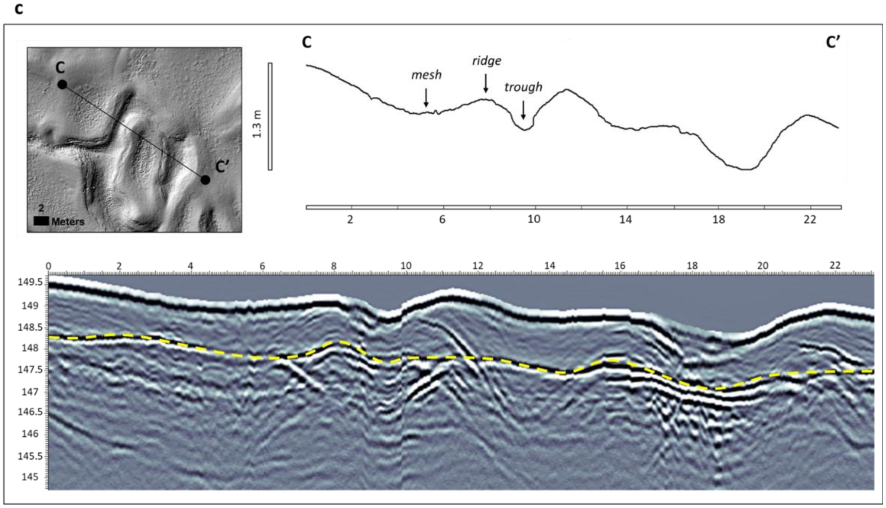
C
C'
2
Meters
mesh
ridge
trough
1.3 m

Figure 6: LiDAR Hillshade, LiDAR-derived topographic profiles and GPR transects of VRFs. Transect locations can be found in Figure 5. Units in meters. Maximum vertical relief on the y-axis of topographic profiles. Elevation is on the y-axis of GPR transects. (a) Line 1 (A-A'), (b) Line 2 (B-B') and (c) Line 3 (C-C') topographic profiles demonstrate a mesh-ridge-trough sequence. VRF troughs are pointed to bowl-shaped concave depressions. Yellow dashed line in GPR transects represents thaw depth (i.e., depth to permafrost in July 2019). Bright reflectors can be seen beneath closed cell VRF central troughs indicating the presence of ice. These reflectors demonstrate a wedge-shaped object (shaded in yellow) in Lines 1 and 2.

Well-developed polygons are also present at the main field site. Polygons range in diameter (long axis) between 115 and 167 m, and trough width averages around 3 m, but can reach up to nearly 6 m. Thin and narrow secondary troughs are present within the larger polygon centers (Fig. 5). Secondary troughs propagate from a major trough and often terminate within the polygon center (Fig. 5). Polygon troughs appear to typically cross-cut VRFs but can also merge with VRFs to create an anastomosing ensemble of ridges and troughs (Figs. 3 and 5).

VRF morphology varies laterally and with elevation among the terraces. The main field site is characterized by more mounds down valley (Fig. S1a, Supp. Files) and less mounds with high-center polygons exposing the VRF-containing deposit up valley (Fig. S1d, Supp. Files). Additionally, the uppermost terrace has a thin VRF-containing deposit that appears degraded (i.e., subtle hummocks, thin deposit, less pronounced morphology) (Fig. S1e, Supp. Files) relative to VRFs on neighboring, lower terraces that appear to reside in much thicker deposits (Fig. S1b,f, Supp. Files). Additionally, more vegetation is present at the main field site (Fig. S1c,d, Supp. Files) compared to the other terraces (e.g., Fig. S1a,b,e,f, Supp. Files).

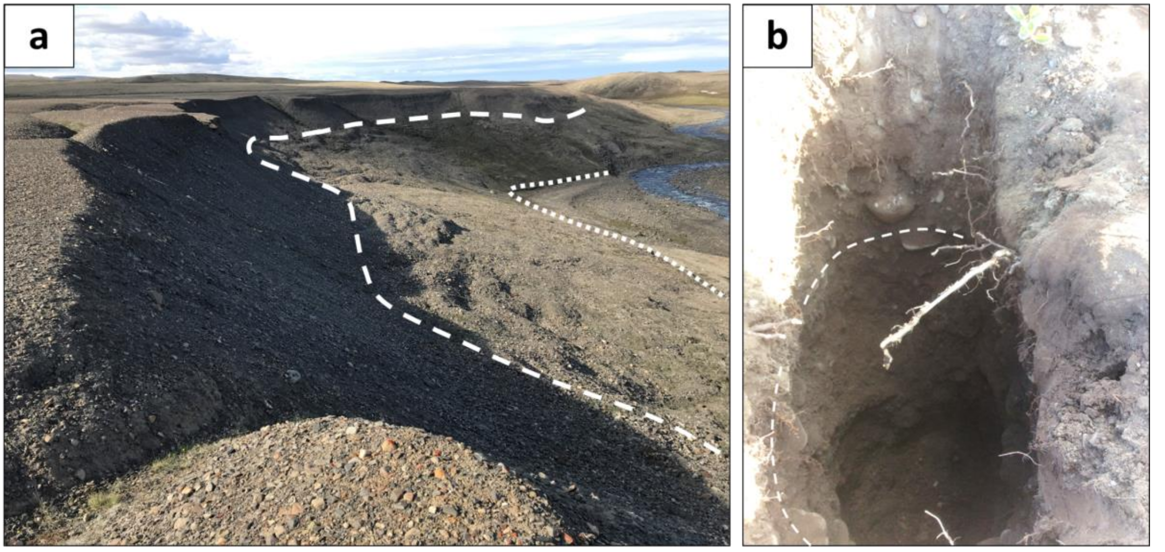

Figure 7: Characteristics of VRF materials at river cutbank. (a) River cutbank exposing deposit thickness (Location identified in Figure 2). Polygons are visible at the top of the deposit. The surface to the white dashed line is characterized by a steep talus slope ~ 6 m thick. A gently sloped section of lobate material occurs between the white dashed line and the white dotted line. Below the white dotted line is a river sand bank. (b) Pit dug 89 cm into the main field terrace. White dashed line outlines flat-oriented gravel.

Three GPR transects were collected at the main field site. Lines 1, 2, and 3 cross over closed-cell VRFs (Figs. 5 and 6) and show a thaw depth (July 2019) ranging between 1 and 1.5 m that can be identified by a nearly continuous bright linear reflection below the surface (Fig. 6). Stacked bright radar reflections are observed below the central depression of a close-cell ridge at Lines 1 and 2 (Fig. 6). Line 3 shows bright reflections beneath two troughs adjacent to a closed-cell ridge. However, the center of the closed-cell ridge at Line 3 does not appear to have an obvious bright reflection. Deposit thickness is indeterminate in the GPR transects, suggesting the deposit thickness exceeds the signal penetration depth of approximately 4 m. VRFs were also observed directly on top of thaw slumps across the field region, which exposed deposits as thick as 10 to 15 m.

5 Discussion

We have documented a landform, referred to here as Vermicular Ridge Features (VRFs), northwest of Mokka Fiord on Axel Heiberg Island, Nunavut, Canada. These features exhibit a circular, elongated, sinuous, and/or anastomosing series of ridges and troughs (Figs. 3 and 5) and are near-identical to features documented on the south coast of Devon Island (Hibbard et al., 2021). Below, we compare VRFs on Axel Heiberg Island to other morphologically similar periglacial and glacial landforms, namely lithalsas and morainic rim ridges, to better elucidate an origin (Table 1).

5.1 Periglacial Origins

Patterned ground is a common product of periglacial processes that can result in conspicuous morphologies such as circular, sinuous, and anastomosing ridges and troughs. Stone circles are a common periglacial feature that exhibit this morphology and can be found in high and low Arctic regions (Washburn, 1956; Schmertmann and Taylor, 1965; Washburn, 1973; Hallet and Prestrud, 1986; Hallet, 2013). Stone circles are characterized by their circular to labyrinthine coarse-grained ridges surrounding a central fine-grained domain. Ridge width typically ranges between 0.5–1 m and ridge height usually reaches up to 0.5 m, with circle diameters ranging between 2–5 m (Hallet and Prestrud, 1986; Kessler et al., 2001; Hallet, 2013). Stone circles also commonly exhibit cracks along the axial trace of circular ridges that form from frost heave and soil upwelling (Kääb et al., 2014). However, while the scale is similar, no grain sorting or evidence of soil upwelling was observed in the Mokka Fjord VRFs and the microtopography does not reflect that of stone circles. Thus, the properties of the Mokka Fjord VRFs are inconsistent with being stone circles.

Collapsed pingos, palsas, and lithalsas (Table 1), also referred to as circular ramparts or ramparted depressions, and other frost mounds and blisters are periglacial landforms that can also result in circular raised ridge features (Table 1) (Mackay, 1998 and references therein). Pingos are perennial ice-cored hills produced by injection of groundwater under artesian pressure (Holmes et al., 1968; Müller, 1962) or by pore-water expulsion resulting from permafrost aggradation in a water-saturated sandy sediment, such as a shallow lake (Mackay, 1998). Pingos are much larger in scale and typically occur singularly (Table 1) and, therefore, are not comparable to the VRFs at Mokka Fjord; however, can shed light on High Arctic hydrological processes that may lead to VRF formation. For example, the outflow of perennial subpermafrost springs feeds pingo formation across Svalbard (Demidov et al., 2022), possible sub and intra permafrost water flow from nival and/or buried ice melt in Greenland (Allen et al., 1976), glacial meltwater recharge, or deep groundwater injection (Henkemans, 2016).

Table 1: Periglacial and glacial ring ridge feature morphometrics compared to Mokka Fjord VRFs. Modified from Hibbard et al. (2021).

Table 1. Periglacial and glacial ring ridge feature morphometrics and characteristics compared to Mokka Fjord VRFs. Modified from Hibbard et al. (2021).

Name	*Location*	*Age of Formation (ka BP)*	*Diameter*	*Height*	*Ridge Material*	*Formation Mechanism*	*Reference*
This study							
Vermicular Ridge Features (VRFs)	Axel Heiberg Island, Nunavut, Canada	≤ 10	6–37 m	up to 1.5 m	clast rich sandy glaciofluvial sediment and till	ice marginal glaciofluvial and supraglacial origin, dead ice ablation	This study
Periglacial in Origin							
Pulkijärvi rim ridges	northern Finland	< 9–10	50–150 m	0.5–4.5 m	unstratified poorly sorted sandy till	collapsed open system pingo-like frost mounds (i.e., lithalsa)	Seppälä, 1972
Circular lakes	northern Norway	> 1.5	up to 40 m	up to 1.5 m	fine grained glaciofluvial deposits with peat lenses	collapsed minerogenic frost mounds (i.e., lithalsa)	Svensson, 1969
Ground ice depressions	East Anglia, UK	11	10–120 m	up to 5 m	fine chalk rubble and sand with thin organic lenses	collapsed frost mound/thermokarst degradation	Sparks et al., 1972
Remains of pingos	Southwest Wales, UK	–	60–165 m	can exceed 10 m	clay silt and gravelly clay	collapsed open system pingos	Watson and Watson, 1974 (same feature described by Ross et al., 2019)
Palsa-like mounds	northern Sweden	–	4–40 m	1–2 m	silty/clayey material with a high block content in blocky only	collapsed palsa-like frost mounds	Åkerman and Malmström 1986; Rapp and Rudberg, 1960
Palaeo thermokarst depressions	South Bohemia, Czech Republic	14–16	up to 120 m	up to 6 m	sandy gravel	collapsed lithalsas subsequently filled with lake basin sediments	Hošek et al., 2019
Viviers/lithalsa remnants	eastern Belgium	11–13	up to 200 m	< 1 m, up to 8 m	clayey silt with pebbles and peat	collapsed lithalsas	Pissart, 2003 and references therein
Pingo/lithalsa remnants	southern Ireland	10–11	50–100 m	1–2 m	coarse sand and frost shattered pebbles	collapsed lithalsas	Coxon, 1986; Coxon and O'Callaghan, 1987; Pissart, 2003
Decayed lithalsa	Umiujaq, Nunavik, Northern Québec	0.1–1.5	50 m	2–3 m	silt and clay layer overlying sand and gravel layer	eroded palsa, now lithalsa at initial stage of degradation/collapse	Calmels et al., 2008
Ice-cored depression	southern Netherlands	~14–18	up to 90 m	3 m	sandy material	collapsed pingo/lithalsa	Kasse and Bohncke, 1992
Lithalsas	Northwest Territories, Canada	0.7	10–120 m	0.3–8 m	silt, clay, and sand	degraded and collapsed lithalsas	Wolfe et al., 2014
Glacial in Origin							
Ring ridge moraines	Devon Island, Nunavut, Canada	< 8	4–72 m	up to 2.5 m	clast rich sandy till	supraglacial origin, dead ice ablation	Hibbard et al., 2021
Hummocky terrain	north-central Alberta, Canada	11–13	—	2–10 m	sandy silt/silty clay with 5–10% clast till	subglacial squeezing	Paulen and McClenaghan, 2014
Pulju Moraines	Finland	9–10	50–100 m	< 1.5 m; 1.6–2.1 m	gravelly to sandy and silty till	subglacial squeezing	Sutinen et al., 2014
Circular Ridges	Norway	~14	50–100 m	2.5–10 m	clast rich sandy till	supraglacial origin, dead ice ablation	Knudsen et al., 2006
Ramparted Depressions	Wales	–	60–165 m	can exceed 10 m	clayey silt and occasional clasts; glacial diamict and glaciolacustrine sediments	either supraglacial or subglacial	Ross et al., 2019 (same feature described by Watson and Watson, 1974)
Veiki Moraines	Sweden	< 11–12	100s of m	4–10 m	clay, silt, sand, gravel	subglacial and supraglacial origin	Lagerbäck, 1988
Ring Ridge Hummocky moraines	northern Finland	–	20–200 m	0.5–4 m	sandy silty till with some gravel and with boulders on ridges overlying clay-rich till	supraglacial origin, dead ice ablation	Aartolahti, 1974
Ice Contact Rings	Saskatchewan, Canada	–	10s of m	1.5–10.5 m	till, sand and gravel	supraglacial origin, dead ice ablation	Parizek, 1969
Type 2a Hummocks	Russia	–	1–50 m	–	diamicton	englacial origin, dead ice ablation	Boyes et al., 2021, 2024
Circular moraine features (CMF)	northern Norway	11–13	20–170 m	0.3–10 m	diamicton	englacial origin, dead ice ablation	Ebert and Kleman, 2004

Lithalsas are smaller scale frost mounds that form by ice segregation in mineral-rich soil absent of peat and can be found on river terraces and along streams. They form through permafrost aggradation causing localized ice segregation as pore water migrates (Calmels et al., 2008). The formation of lithalsas requires specific environmental conditions in order to allow slow freezing times to promote cryosuction for ice lens growth. The limited examples of contemporary lithalsas appear to be restricted to the discontinuous permafrost zone with available groundwater supply and in frost susceptible fine-grained sediment as opposed to the coarser grained sediments like what we observe in our study area (Calmels et al., 2008; Wolfe et al., 2014); although others have proposed lithalsa remnants to be present in coarse-grained materials (e.g., Rapp and Rudberg, 1960; Seppala, 1972; Akerman and Malmstrom, 1986; Coxen, 1986; Hosek et al., 2019). More importantly, Mokka Fjord VRFs are located in the continuous permafrost zone and have been in a polythermal and cold glacial environment with little water supply since the retreat of the Innuitian Ice Sheet (Ó Cofaigh et al., 1999). Palsas and lithalsas are argued to occur in areas where water is abundantly available and not limited to a shallow active layer (Pissart, 2002) as would be expected in the continuous permafrost zone. It is argued that only seasonal or short-lived frost mounds and blisters could form in the continuous permafrost zone due to limited hydrostatic conditions (French, 1971; Morse and Burn, 2014). Therefore, the strict environmental conditions necessary for lithalsa formation would not readily have been met at Mokka Fjord. However, Paquette et al. (2020) argued that small lithalsa plateaus formed in the high arctic near Resolute Bay, Nunavut, Canada in a shallow wetland. They suggest ice aggradation can slowly heave the bottom of wetlands upwards, eventually exposing water-saturated materials to air temperatures leading to permafrost aggradation and ice lens formation. To the authors knowledge, this is the only example of a possible contemporary high arctic lithalsa that Paquette et al. (2020) argue is only possible due to the sustained water supply provided by the wetland setting. Mokka Fjord VRFs reside in a floodplain which may experience occasional, or maybe even frequent, flooding depending on Holocene climate. Yet, this would not provide the sustained water supply that a wetland provides. Additionally, VRFs at Mokka Fjord exhibit a much more complex morphology than has been observed in remnant and contemporary lithalsas (Fig. 3), which tend to be circular ramparts.

Other segregation ice landforms display a much more similar morphology to Mokka Fjord VRFs. The Involuted Hill sites located in Tuktoyaktuk, Northwest Territories, Canada, exhibit a similar, yet not identical, complex morphology as observed in Mokka Fjord VRFs. The Involuted Hills are clay till-mantled ice-cored hills with a series of ridges and troughs. The ridges there are approximately 10 to 40 m wide, several tens of meters in length, and up to 6 m in height (Mackay, 1963; Rampton, 1988; Mackay and Dallimore, 1992). Mackay and Dallimore (1992) suggest glacial meltwater and porewater expulsion are what led to the formation of the massive ice at Involuted Hill, and that differential degradation of that ice led to the series of ridges and troughs at the surface. Although this morphologically similar, albeit larger, landform is found at lower latitudes than Mokka Fjord, providing more opportunity for talik formation and permafrost aggradation, smaller pingo-like frost mounds and partially collapsed mounds have been documented in the Canadian high arctic on Banks Island, Northwest Territories. These are suggested to form from the freezing of fluvial taliks left over from previous lateral stream migration (Pissart and French, 1976, 1977). Furthermore, pingos in Svalbard have been suggested to form from the infiltration and migration of polythermal glacial meltwater to taliks (Liestøl, 1977). However, these are isolated frost mounds, unlike what is observed at Mokka Fjord.

These examples of frost mounds demonstrate the diversity of environmental conditions, water availability, and morphology/morphometry observed across ice segregation features. Mokka Fjord VRFs occur within a fluvial/glacio-fluvial setting that has sediments conducive to the upward and lateral movement of groundwater. Therefore, Mokka Fjord VRFs could have formed from the freezing of glacial meltwater taliks in fluvial/glacio-fluvial sediments and/or till due to permafrost aggradation following glacial retreat. However, taliks generally form in deep bodies of water (~1.5-2 m) such as beneath lakes or large rivers (Mackay et al., 1998; Jorgenson and Shur, 2007; Arp et al., 2011). The meltwater channels at Mokka Fjord may not have penetrated deep enough to lead to talik formation; however, the presence of a nearby salt dome (Mokka Fiord Diapir – See Fig. 2) may depress the freezing point and potentially contribute to more susceptible talik formation in the area (e.g., Mackay et al., 1998). Additionally, if an environment conducive to increased water output from the high arctic glaciers existed, then ice-walled lakes or occasional glacial outburst flooding could potentially lead to talik formation. Permafrost aggradation would lead to segregated ice formation which could form lithalsa plateaus and/or frost mounds. This would be followed by the differential ablation of buried ice and redistribution of mantling sediment leading to the formation of a series of ridges and troughs (see Figure 12 from Hibbard et al., 2021).

Although we have not entirely ruled out periglacial origins, Axel Heiberg Island lies within a recently deglaciated landscape where large amounts of dead glacial ice are likely preserved in the continuous permafrost zone under the protection of surface debris cover (Coulombe et al., 2019; O'Neill et al., 2019). Morphologically similar features can form from the ablation of buried glacial ice as well as from other glacial-related processes (discussed in the next section). Therefore, we consider possible glacial formation mechanisms and analogous landforms to compare to Mokka Fjord VRFs.

5.2 Glacial Origins

Ring ridges (a general non-genetic term used to encompass the variety of naming schemes used in the literature) are glacially-derived circular to anastomosing raised-ridge features found largely across northern Europe and North America (Table 1). Although ring ridge origins remain debated, their formation is largely attributed to one of the following two main hypotheses: (1) Supraglacial debris concentrations left from the disintegration of stagnant proglacial/ice-marginal ice, including HT type 2 hummocks in Albera, Canada (Evans et al., 2014), Circular Ridges in Norway (Knudsen et al., 2006), Ring Ridge Hummocky moraines in Finland (Aartolahti, 1974), Ice-contact Rings in Saskatchewan, Canada (Parizek, 1969), ring ridge moraines in Nunavut, Canada (Hibbard et al., 2021), and more (Boulton, 1967; Clayton, 1967; Clayton and Moran, 1974; Eyles, 1979, 1983; Kruger , 1983; Paul, 1983; Clayton et al., 1985; Sollid and Sorbel, 1988; Johnson et al., 1995; Ham and Attig, 1996; Patterson, 1997, 1998; Jennings, 2006; Schomacker, 2008; Evans, 2009); (2) Subglacial diapirism and squeezing of subglacial water-saturated till into basal cavities of disintegrating glacial ice leaving subglacial till ring ridges, including hummocky terrain in Alberta, Canada (Paulen and McClenaghan, 2014), and Pulju moraines in Finland (Sutinen et al., 2014, 2018, 2019; Middleton et al., 2020), and more (Hoppe, 1952; Eyles et al., 1999; Stalker, 1960; Boone and Eyles, 2001; Menzies and Shilts, 2002). Other suggested formation hypotheses include (1) forming from either (Gravenor and Kupsch, 1959; Watson and Watson, 1974; Ross et al., 2019); (2) both (Lagerbäck, 1988) supraglacial and subglacial origins; (3) englacial origins (Ebert and Kleman, 2004; Boyes et al., 2021; 2024); (4) from ice blocks settling and melting in a drained proglacial or ice-marginal lake leaving predominantly fine-grained till and lacustrine sediments (Dionne, 1978; Mollard, 2000); (5) subglacial meltwater erosion similar to that of drumlins and Rogen moraines, and other transverse moraines (Shaw, 1996; Munro-Stasiuk and Shaw, 1997; Munro-Stasiuk and Sjogren, 2006); and (6) proglacial extrusion of sediment due to over-pressurized groundwater (Bluemle and Clayton, 1984; Bluemle, 1993; Boulton and Caban, 1995; Evans et al., 1999). More details regarding the various types ring ridges and their specific differences are described in Johnson and Clayton (2003) and Hibbard et al. (2021).

There is considerable variation in the scale, landform association, and sedimentology of ring ridges (Table 1), yet many are found in farmland and vegetated regions, which likely leads to the preferential preservation of large-scale landforms, and only a handful are composed of coarse-grained sediment (Table 1). Mokka Fjord VRFs are small-scale and occur in course-grained sediments. Additionally, the morphometry, affiliated ice sheet characteristics, and thermal regime (i.e., Innuitian, Laurentide, British-Irish, vs. Fennoscandian Ice Sheets), and/or deposit age of ring-ridges differ markedly from the Mokka Fjord VRFs (Table 1). Only the Dundas Harbour ring-ridge moraines (Hibbard et al., 2021) are comparable in both morphometry and sedimentology to Mokka Fjord VRFs among other coarse-grained glacially derived ring ridges (Table 1).

Importantly, ring ridges at Dundas Harbour (Hibbard et al., 2021) are identical in morphology and morphometry to the VRFs at Mokka Fjord. For example, individual circular closed-cell VRFs on Dundas Harbour (Devon Island) and Mokka Fiord (Axel Heiberg Island) exhibit an identical microtopography consisting of rounded convex ridges, a u-shaped concave central depression with an abrupt change in slope at the ridge-trough transition, miniature grooves where cracks along the ridge apex occur, and gradual outward-facing slopes leading to the mesh (Fig. 8). The sedimentology of ring ridges at Dundas Harbour was interpreted as a sandy clast-rich till based on grain size analyses (Hibbard et al., 2021). Although no grain size distribution was done on Mokka Fjord VRFs, extensive field observations indicate the material is composed of sub-rounded clast-rich sand and shows minor evidence of preferred orientation and minimal stratification of sands and gravels in the pits dug and exposures observed in the field. The sedimentology at Mokka Fjord is most consistent with a glaciofluvial deposit rather than a glacial till.

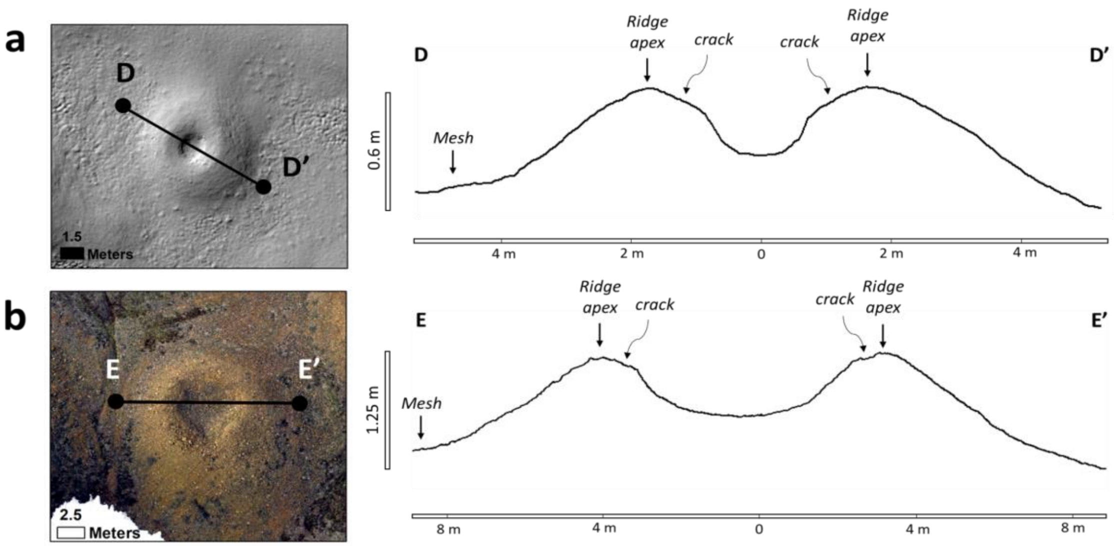

Figure 8: Topographic profiles of circular closed cell VRFs at Mokka Fiord and Dundas Harbour. (a) Example of circular VRF at Mokka Fiord, Axel Heiberg Island, Nunavut, Canada (D-D'). LiDAR data on the left and topographic profile on the right. VRF displays rounded convex ridges with cracks running just off the axial trace of the ridge, a u-shaped central trough following an abrupt change of slope from the ridge cracks, and a gently sloping transition into the mesh. (b) Example of circular VRF at Dundas Harbor on Devon Island, Nunavut, Canada (E-E'). Aerial drone imagery on the left and topographic profile on the right. VRF displays the same microtopography observed in (a) with a larger diameter. Modified from Hibbard et al. (2021).

It is notable that thermal contraction crack polygons are observed at Mokka Fiord and clearly cross-cut the VRFs indicating post-depositional modification of the VRF materials (Figs. 3, 5, S1, Supp. Files). This relationship is also observed at Dundas Harbour (Hibbard et al., 2021). However, polygons at the main Mokka Fiord field site are much more developed and well defined compared to those at Dundas Harbour. For example, the polygon troughs are wider, have raised shoulders with cracks running parallel to the troughs, and have both primary and secondary troughs with ice wedges. In addition to ice-wedge polygons, Mokka Fiord has exposed ice at active thaw slumps, whereas no evidence for massive buried ice was observed at Dundas Harbour. This may be the product of more ice (and therefore more water) in the region and longer subaerial exposure at Mokka Fiord as the field site is much farther away from the ice caps compared to the ring ridges located at Dundas Harbour (Hibbard et al., 2021). Therefore, despite their identical morphology and morphometry, the depositional environment was different at Mokka Fjord and Dundas Harbour. Which begs the question, are ring ridges at Dundas Harbour the same as VRFs at Mokka Fjord or are their similarities a product of equifinality suggesting that different processes can lead to a similar geomorphic expression? And, if so, what are the processes involved? More importantly, do (or could) Mokka Fjord VRFs have glacial origins?

Bednarski (1998) describes the Quaternary geomorphology and stratigraphy of northeastern Axel Heiberg Island, which is ~300 km northeast of our field site at Mokka Fiord and lies within the outwash plains emanating from the Princess Margaret Range. The outwash plains described by Bednarski (1998) are reported to host extensive kettled outwash terraces (also referred to as kettled sandar) and kame terraces. Kettled/pitted sandur (sandar, plural) are glacial outwash plains composed of glaciofluvial deposits with kettle holes that resulted from the burial and subsequent melting of stranded glacial ice. Sandar can be ice-marginal and extend into a distal outwash proglacial setting. Stagnant detached glacial ice can be found buried beneath glaciofluvial sediments and till in an ice-marginal setting.

Kame terraces are ice-marginal/ice-contact features that form alongside meltwater channels and are in contact with glacial ice. They can be easily confused with fluvial or outwash terraces (i.e., sandar) (Menzies, 2002). However, kame terraces typically have multiple steps/terraces on one side of a channel that have varying gradients and elevations to terraces on the opposite side of the channel (e.g., Gray, 1975; Sissons, 1982). Kame terraces are mostly composed of glaciofluvial sands and gravels from lateral meltwater channels; however, supraglacial and englacial till can accumulate on top of glaciofluvial sediments (e.g., Levson and Rutter, 1989). It is common for kame terraces to bury and preserve remnant glacial ice (e.g., Mckenzie, 1969; McKenzie and Goodwin, 1987). Kame terraces are often associated with kettle and kame topography, hummocky moraines, and eskers (Benn and Evans, 2010).

The kettled outwash/kame terraces described by Bednarski (1998) are reported to be composed of ice-contact glaciofluvial coarse gravel with kettles and kames that range from 30−50 m in relief, ice-contact ridges, and active slumping that indicate the presence of buried glacial ice. Therefore, buried "dead" ice can be found and associated with both kame terraces and sandar. Additionally, ice blocks can become stranded in a kame terrace or outwash plain which can act as an obstacle for glaciofluvial sediment to accumulate around or can become completely buried (e.g., Russell et al., 2006). However, the transport of ice blocks to more distal sandur is possible via glacial meltwater channels (Maizels, 1977) and/or glacial outburst floods (Fay, 2002). Therefore, ice blocks can be transferred to and deposited within floodplains on sandar. VRFs at Mokka Fjord are found on both terraces and within the floodplain which could be explained by a kettled outwash/kame terrace origin.

Kame terraces are also suggested to be present along the west coast of Flat Sound (Fig. 1), close to Mokka Fjord, where a northwest-flowing trunk glacier in Nansen Sound was in contact with the eastward-flowing glaciers from the Axel highlands (Bednarski, 1998). The proximity and similarity in observations between those described by Bednarski (1998) and in this study suggest that Mokka Fjord VRFs may be the product of ice-marginal processes with coarse-grain material supporting a low-transport more proximal setting. VRFs at Mokka Fjord could, therefore, result from the ice-marginal deposition of glaciofluvial sediment over dead glacial ice and/or supraglacially buried detached ice, rather than strictly from a morainic origin as suggested for VRFs at Dundas Harbour (Hibbard et al., 2021). Following the detachment of ice and deposition of ice-marginal material, differential ablation led to the formation of the conspicuous ridges and troughs that are currently undergoing periglacial modification.

The difference in scale and morphometry to other documented ring-ridges (Table 1) is likely due to the preservation bias of small-scale features on a largely uninhabited and unvegetated landscape that formed more recently compared to the older ring-ridge moraines that occur at lower latitudes.

5.3 Proposed Origin of Mokka Fjord VRFs

We consider two plausible formation mechanisms for Mokka Fjord VRFs: a periglacial origin (i.e., segregation ice features/lithalsas) and a glacial origin (i.e., ring-ridge moraines and kettled outwash/kame terraces) (Fig. 9). A common concept in both glacial and periglacial geomorphology is equifinality (Möller and Dowling, 2018), where different processes can lead to similar landforms, making process history necessarily ambiguous. We suggest that both hypotheses involve the initial preservation and eventual degradation of buried ice to produce the observed VRFs at Mokka Fjord. However, the mechanisms of ice preservation differ significantly, with distinct implications for the climatic and environmental conditions under which they formed. Based on these hypotheses, we explore the environmental conditions, ice sheet thermal regime, and timing of deposition, preservation, and degradation necessary to produce Mokka Fjord VRFs (Fig. 9).

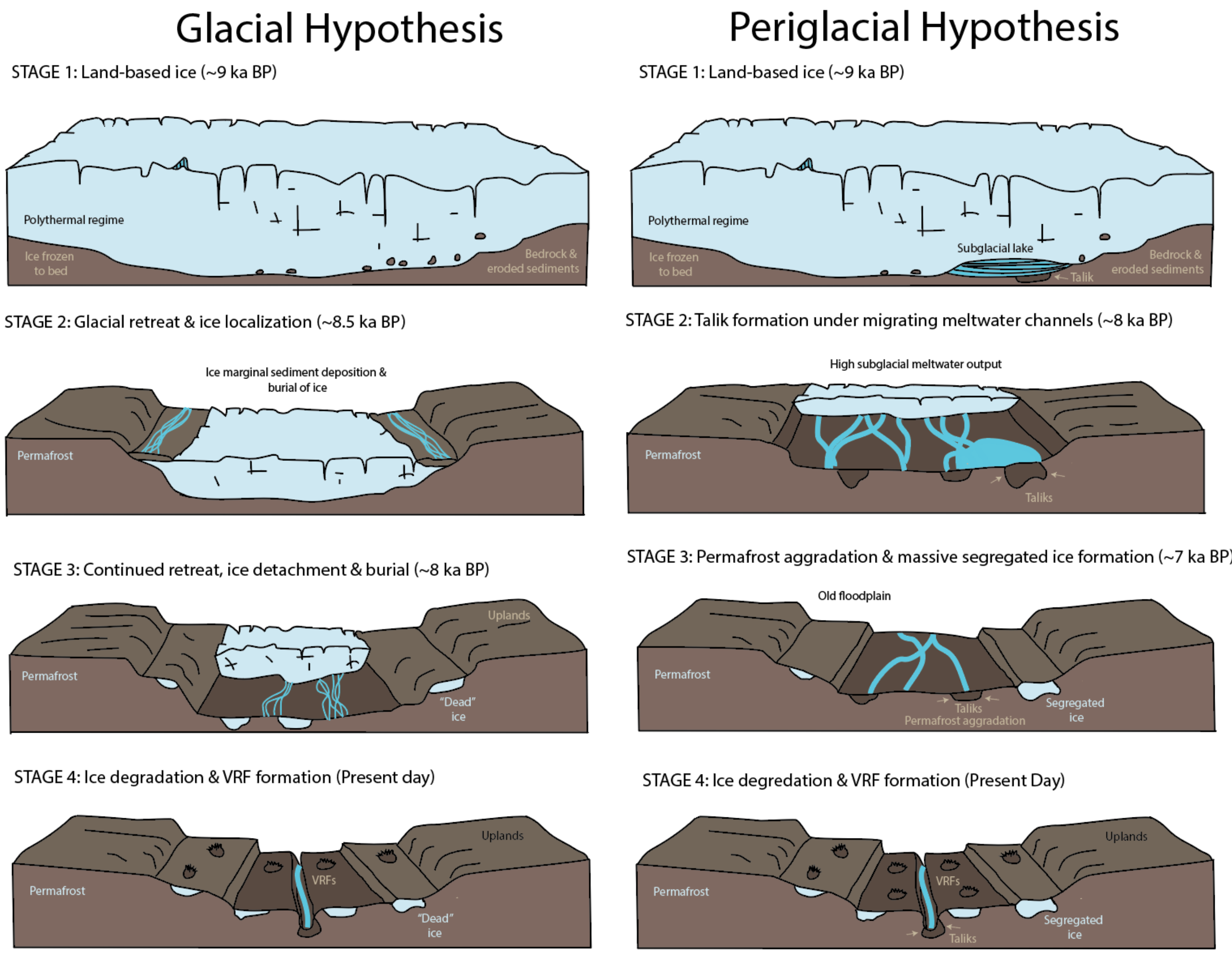

Figure 9: A simplified landscape evolution model for our two proposed Mokka Fjord VRF formation mechanisms. *Glacial:* Stage 1 depicts the study area covered by land-based ice around 9 ka BP (based on England et al, 2006), within a polythermal glacial environment. Stage 2 shows the progressive thinning and recession of land-based ice, with ice occupying topographic lows. During this stage, supraglacial till and glaciofluvial runoff deposit sediments and bury ice margins, which promotes ice detachment from the main body. Stage 3 highlights continued retreat and the detachment and burial of "dead" glacial ice in the outwash plains and ice marginal kame terrace remnants. Stage 4 presents a mature meltwater channel system with remnant buried "dead" glacial ice. The continued degradation of buried ice results in VRF formation (starting prior to Stage 4). Concurrently, periglacial processes further modify the landscape. *Periglacial:* Stage 1 depicts the study area covered by land-based ice around 9 ka BP (based on England et al., 2006), within a polythermal glacial regime. Periods of warming and/or localized warm-based thermal regimes may lead to subglacial lakes and talik formation. Stage 2 shows the progressive thinning and recession of land-based ice, with ice occupying topographic lows. Periods of high water output will be necessary to form deep water bodies for talik formation. Channel migration and lake drainage will lead to freezeback of taliks. Slow permafrost aggradation will lead to massive segregated ice formation. Stage

3 features fluvial terraces forming. Migrating channels create new taliks followed by freezeback. Stage 4 presents a mature meltwater channel system. Remnant segregated ice continues to degrade and form VRFs (starting prior to Stage 4). Periglacial processes continue to modify the landscape alongside the ongoing VRF formation. Modified from Flint, 1971.

The thermal regime of glaciers on Axel Heiberg Island today are cold and polythermal (Blatter, 1987; Ó Cofaigh et al., 1999) which is thought to have extended into the last glacial maximum, except for fjord glaciers, which are interpreted to be warm-based glaciers, and ice streams (England et al., 2006; Ó Cofaigh et al., 1999). There is minimal evidence of wet-based glaciation on the island, with only minor evidence of striated bedrock and erratic dispersal trains resulting from localized warm-based conditions (Ó Cofaigh et al., 1999), supporting a largely polythermal/cold thermal regime with occasional warming events.

Marine-based ice largely disappeared by 9 ka BP, leaving mostly land-based ice on Axel Heiberg and other islands (England et al., 2006). At this point, our field site near Mokka Fjord would have been overlain by ice (Fig. 9 - Stage 1). A glacial VRF interpretation assumes a largely polythermal environment throughout the Holocene (Fig. 9 - Glacial Stage 1). As land-based ice continued to thin and recede (Fig. 9 - Glacial Stage 2), ice would preferentially occupy topographic lows and supraglacial till and glaciofluvial runoff would deposit sediment and bury ice margins, facilitating ice detachment from the main body. Continued recession leaves detached buried "dead" glacial ice in the outwash plains and ice marginal terraces, such as buried ice blocks or detached snout or marginal ice (Fig. 9 - Glacial Stage 3). Over time the remnant buried "dead" glacial ice will degrade and begin to form VRFs and periglacial processes will overprint and modify the landscape that continue to present day (Fig. 9 - Glacial Stage 4).

A periglacial interpretation would imply periods of warming, as sufficient water supply for talik formation and water injection would be necessary. Therefore, periods of warming or localized warm-based glacier conditions could result in subglacial lakes hosting local taliks (Fig. 9 - Periglacial Stage 1). As land-based ice continued to thin and recede (Fig. 9 - Periglacial Stage 2), periods of high water output would be necessary to form deep enough water bodies for talik formation beneath them. However, the inclusion of salts from the nearby Mokka Fjord Diapir may form taliks more readily in a normal polythermal environment. Channel migration and lake drainage will lead to freezeback of taliks. Slow permafrost aggradation will lead to massive segregated and injection ice formation. The inclusion of salts may reduce the rate of freezeback allowing for massive ice formation. Migrating channels continue to create new taliks followed by freezeback and massive ice formation (Fig. 9 - Periglacial Stage 3). Over time the remnant buried segregation ice will degrade and begin to form VRFs and other periglacial processes will overprint and modify the landscape that continue to present day (Fig. 9 - Periglacial Stage 4).

While both proposed mechanisms are capable of forming the Mokka Fjord VRFs, the periglacial mechanism is more complex due to its stricter timing and thermal constraints compared to a simpler glacial origin. Land-based ice on Axel Heiberg Island deglaciated to its near-present extent between 9 and 7.5 ka BP (England et al., 2006). Therefore, talik formation and freezeback, and massive ice formation and degradation would need to occur in less than 1,500 years for Mokka Fjord VRFs to form. The rate of talik formation and freezeback is currently debated, which will influence the formation of massive segregated ice. Burn (2002) estimated talik development under bodies of water > 4m in the continuous permafrost zone may take 3500-9000 years to form. Others have suggested it would take thousands of years to develop ice rich permafrost following land exposure (Jorgenson et al., 1998). Therefore, it could take >1,500 years to develop and freezeback a talik. Yet, Stephani et al. (2019) found that permafrost growth in northern Alaska occurred at a rapid rate (~6-34 years) in land exposed following channel migration. Additionally, the Illisarvik Drained Lake Experiment demonstrated both permafrost growth and pingo formation within 35 years following lake drainage (Mackay and Burn, 2002; French, 2017) and have been suggested by others to form on the order of ~5-1000 years (Mackay, 1998; Samsonov et al., 2016). Therefore, it may be possible for VRFs to form from frost mound processes, but the depositional environment would also need to remain proximal to the glacier to maintain a coarse-grained glaciofluvial environment, limiting the timeframe for talik and ice segregation formation. Additionally, the added complexity of talik formation necessitates a greater water supply to form deeper water sources or possibly the addition of salts to depress the freezing point of the permafrost. Nival and/or buried glacial ice melt may also be considered.

A glacial origin would simply require the thinning, detachment, and burial of marginal ice in a glaciofluvial setting, either in a supraglacial or proglacial environment. Following Occam's Razor, the principle of parsimony, which suggests that the simplest explanation requiring the fewest assumptions is usually correct, we propose that the Mokka Fjord VRFs most likely formed from the burial and eventual detachment of ice-marginal/snout glacial ice, followed by differential ablation of ice. This mechanism is similar to that suggested for ring ridge moraines at Dundas Harbour (Hibbard et al., 2021).
While we do not rule out the possibility that the Mokka Fjord VRFs could have formed as localized frost mounds or other segregation ice mounds, we consider it a more complex scenario requiring more assumptions. Hence, the glacial hypothesis is our preferred interpretation.

6 Summary and Conclusions

Vermicular Ridge Features (VRFs) at Mokka Fjord exhibit a circular, elongated, sinuous, and/or anastomosing morphology as a series of ridges and troughs. They occur along terraces and within the floodplain of a glacial meltwater channel. Thaw slumps (Fig. 4), active lobate slumping (Fig. 7), and thermokarst degradation (Fig. 3e) found among the VRFs suggest the presence of buried massive ice underneath. However, the origin of this ice is not known.

The leading periglacial (i.e., segregation ice features/lithalsas) and glacial (i.e., ring-ridge moraines and kame/kettled terraces) origins (Fig. 9) discussed above for Mokka Fjord VRFs all involve buried massive ice and the differential ablation of that ice to form the resulting surface topography and morphology. As the ice melts, the overlying deposit redistributes to preferentially promote a hummocky surface, like the process described by Hibbard et al. (2021) for identical features on Devon Island. Hence, the process of debris-mantled ice disintegration can form morphologically similar features regardless of the exact mechanism of debris transport and deposition needed prior to VRF formation, and regardless of the ice origin. This presents the ongoing difficulty in distinguishing periglacial and glacial landforms in ice-cored terrain that result in a near identical morphology (e.g., Rampton, 2001; Ross et al., 2019; Dyke and Evans, 2003), and, consequently, the concept of equifinality in geomorphology (e.g., Haines-Young and Petch, 1983; Möller and Dowling, 2018).

Based on our observations, we interpret Mokka Fjord VRFs to be an ice-marginal feature resulting from paraglacial ablation of buried glacial ice producing a hummocky ring-ridge moraine comprised of supra- and englacial debris. This formation mechanism would infer a largely polythermal glacial environment with limited water supply. Likely from occasional warm-based periods at the ice margins which may allow sediment output and ice burial from basal ice debris redistribution or the thinning and subsequent burial of snout ice from glaciofluvial outwash.

Competing Interests

The contact author has declared that none of the authors have any competing interests.

Acknowledgements

We would like to thank the Inuit of the Qikiqtani Region (one of the three regions in the territory of Nunavut). Fieldwork was carried out on their land in Nunavut. We would like to thank the community of Qausuittuq (Resolute Bay) for welcoming us during our stay in the summer of 2019. Logistical support from the Polar Continental Shelf Program (NRCan) is gratefully acknowledged. Funding was provided by a Canadian Space Agency (CSA) Flights and Fieldwork for the Advancement of Science and Technology (FAST) grant and Natural Sciences and Engineering Research Council of Canada (NSERC) Discovery Grant Northern Supplement to GRO. SH was supported by an appointment to the NASA Postdoctoral Program at the Jet Propulsion Laboratory, California Institute of Technology, administered by Oak Ridge Associated Universities under a contract with NASA (80HQTR21CA005). The research was carried out at the Jet Propulsion Laboratory, California Institute of Technology, under a contract with the National Aeronautics and Space Administration (80NM0018D0004). Reference herein to any specific commercial product, process, or service by trade name, trademark, manufacturer, or otherwise, does not constitute or imply its endorsement by the United States Government or the Jet Propulsion Laboratory, California Institute of Technology. The authors would like to thank Academy of Finland (Coe-LaSR, MS-PLS 300066) and Strategic Research Council at the Academy of Finland project "Competence Based Growth Through Integrated Disruptive Technologies of 3D Digitalization, Robotics, Geospatial Information and Image Processing/Computing - Point Cloud Ecosystem (293389/314312)." Geospatial support for this work provided by the Polar Geospatial Center under NSF-OPP awards 1043681 and 1559691 allowed for the use of ArcticDEM data for this project. Figures throughout this article were created using ArcGIS® software by Esri. ArcGIS® and ArcMap™ are the intellectual property of Esri and are used herein under license. Copyright © Esri. All rights reserved. For more information about Esri® software, please visit www.esri.com. We would also like to thank Inuit Tapiriit Kanatami for their map of Inuit Nunangat, which was used for referencing Inuktut geographical terms.

References

Aartolahti, T.: Ring ridge hummocky moraines in northern Finland, Fenn. - Int. J. Geogr. 134, 1974.

Allen, C.R., O'Brien, R.M.G. and Sheppard, S.M.F.: The chemical and isotopic characteristics of some northeast Greenland surface and pingo waters. *Arctic and Alpine Research*, *8*(3), pp.297-317, 1976.

Andersen, D.T., Pollard, W.H., McKay, C.P., Heldmann, J.: Cold springs in permafrost on Earth and Mars, J. Geophys. Res. E Planets 107, 4–1. https://doi.org/10.1029/2000je001436, 2002.

Arp, C. D., Jones, B. M., Urban, F. E. and Grosse, G.: Hydrogeomorphic processes of thermokarst lakes with grounded-ice and floating- ice regimes on the Arctic coastal plain, Alaska, Hydrol. Processes, 25, 15, 2422–2438, doi:10.1002/hyp.8019, 2011.

Balkwill, H.R.: Evolution of Sverdrup Basin, Arctic Canada, AAPG Bull. (American Assoc. Pet. Geol. 62, 1004–1028. https://doi.org/10.1306/c1ea4f86-16c9-11d7-8645000102c1865d, 1978.

Bednarski, J.M.: Quaternary history of Axel Heiberg Island bordering Nansen Sound, Northwest Territories, emphasizing the last glacial maximum, Can. J. Earth Sci. 35, 520–533. https://doi.org/10.1139/e97-124, 1998.

Blatter, H.: On the thermal regime of an Arctic valley glacier: a study of White Glacier, Axel Heiberg Island, NWT, Canada, Journal of Glaciology, 33, 114, 200–211. https://doi.org/10.3189/S0022143000008704, 1987.

Boone, S.J., Eyles, N.: Geotechnical model for great plains hummocky moraine formed by till deformation below stagnant ice. Geomorphology 38 (1), 109–124. https://doi.org/10.1016/S0169-555X(00)00072-6, 2001.

Boulton, G.S.: Modern Arctic glaciers as depositional models for former ice sheets. J. Geol. Soc. Lond. 128 (4), 361–393. https://doi.org/10.1144/gsjgs.128.4.0361, 1972.

Boyes, B.M., Pearce, D.M. and Linch, L.D.: Glacial geomorphology of the Kola Peninsula and Russian Lapland. Journal of Maps, 17, 2, 497–515, https://doi.org/10.1080/17445647.2021.1970036, 2021.

Boyes, B.M., Pearce, D.M., Linch, L.D. and Nash, D.J.: Younger Dryas and Early Holocene ice-margin dynamics in northwest Russia. Boreas, https://doi.org/10.1111/bor.12653, 2024.

Burn, C.R., Tundra lakes and permafrost, Richards Island, western Arctic coast, Canada. Canadian Journal of Earth Sciences, https://doi.org/10.1139/e02-035, 2002.

Calmels, F., Allard, M. and Delisle, G.: Development and decay of a lithalsa in Northern Quebec: a geomorphological history, Geomorphology, 97(3-4), p. 287-299. https://doi.org/10.1016/j.geomorph.2007.08.013, 2008.

Clayton, L.: Karst Topography on Stagnant Glaciers, Journal of Glaciology, 5, 37, 107–112. https://doi.org/10.3189/S0022143000028628, 1964.

Clayton, L.: Stagnant glacier features of the Missouri Coteau in North Dakota. North Dakota Geological Survey Miscellaneous Series. 30, pp. 25–46, 1967.

Clayton, L., Moran, S.R.: A glacial process-form model. In: Coates, D.R. (Ed.), Glacial Geomorphology. SUNY-Binghamton Publications in Geomorphology, Binghamton, NY, pp. 89–119, 1974.

Coulombe, S., Fortier, D., Lacelle, D., Kanevskiy, M. and Shur, Y.: Origin, burial and preservation of late Pleistocene-age glacier ice in Arctic permafrost (Bylot Island, NU, Canada). *The Cryosphere*, *13*(1), pp.97-111, 2019.

Constable, A.J., Harper, S., Dawson, J., Mustonen, T., Piepenburg, D., Rost, B., Bokhorst, S., Boike, J., Cunsolo, A., Derksen, C. and Feodoroff, P.: Climate change 2022: Impacts, adaptation and vulnerability: Cross-chapter paper 6: Polar regions, 2022.

Demidov, V., Demidov, N., Verkulich, S. and Wetterich, S.: Distribution of pingos on Svalbard. *Geomorphology, 412*, p.108326, 2022.

Dyke, A.S., Dredge, L.A., Hodgson, D.A.: North America deglacial marine- and lake-limit surfaces, in: Geographie Physique et Quaternaire. Presses de l’Universite de Montreal, pp. 155–185. https://doi.org/10.7202/014753ar, 2005.

Dyke, A.S. and Evans, D.J.: Ice-marginal terrestrial landsystems: northern Laurentide and Innuitian ice sheet margins. In: Glacial landsystems, Arnold, London, 143–165, 2003.

Ebert, K., Kleman, J.: Circular moraine features on the Varanger Peninsula, northern Norway, and their possible relation to polythermal ice sheet coverage. Geomorphology 62, 159–168. https://doi.org/10.1016/j.geomorph.2004.02.009, 2004.

Embleton, C., King, C. A. M.: Glacial geomorphology. Edward Arnold Publishers Ltd. London, UK, 1975.

Embry, A., Beauchamp, B.: Chapter 13 Sverdrup Basin, in: Sedimentary Basins of the World. Elsevier, pp. 451–471. https://doi.org/10.1016/S1874-5997(08)00013-0, 2008.

England, J., Atkinson, N., Bednarski, J., Dyke, A.S., Hodgson, D.A., Ó Cofaigh, C.: The Innuitian Ice Sheet: configuration, dynamics and chronology. Quat. Sci. Rev. 25, 689–703. https://doi.org/10.1016/j.quascirev.2005.08.007, 2006.

Environment Canada: Canadian Climate Normals 1981–2010 Station Data. Eureka A station, Nunavut. Government of Canada. http://climate.weather.gc.ca/climate_normals/ (accessed 12 June 2021), 2021.

Esri: "Imagery" [basemap]. Scale Not Given. "World Imagery". July 18, 2018. https://www.arcgis.com/home/item.html?id=10df2279f9684e4a9f6a7f08febac2a9. (accessed 20 June 2020), 2018.

Evans, D.J.A.: Controlled moraines: origins, characteristics and palaeoglaciological implications. Quat. Sci. Rev. 28 (3), 183–208. https://doi.org/10.1016/j.quascirev.2008.10.024, 2009.

Evans, D.J., Young, N.J. and Cofaigh, C.Ó.: Glacial geomorphology of terrestrial-terminating fast flow lobes/ice stream margins in the southwest Laurentide Ice Sheet. Geomorphology, 204, 86–113, https://doi.org/10.1016/j.geomorph.2013.07.031, 2014.

Eyles, N.: Facies of supraglacial sedimentation on Icelandic and alpine temperate glaciers. Can. J. Earth Sci. 16, 1341–1361, 1979.

Eyles, N.:Modern Icelandic glaciers as depositionalmodels for ‘hummocky moraine’ in the Scottish Highlands. In: Evenson, E.B., Schluchter, C., Rabassa, J. (Eds.), Tills and Related Deposits. Balkema, Rotterdam, pp. 47–59, 1983.

Eyles, N., Boyce, J.I., Barendregt, R.W.: Hummocky moraine: sedimentary record of stagnant Laurentide Ice Sheet lobes resting on soft beds. Sediment. Geol. 123 (3), 163–174. https://doi.org/10.1016/S0037-0738(98)00129-8, 1999.

Fairbridge, R.W.: Inversion (of topography, relief). In: Geomorphology. Encyclopedia of Earth Science. Springer, Berlin, Heidelberg. https://doi.org/10.1007/3-540-31060-6_193, 1968.

Flint, R.F.: Glacial and Quaternary Geology. Wiley, 1971.

French, H.M.: The periglacial environment. John Wiley & Sons, 139-141, 2017.

French, H.M.: Ice cored mounds and patterned ground, Southern Banks Island, Western Canadian Arctic. Geografiska Annaler Series A, Physical Geography, 53, 32–38. https://doi.org /10.1080/04353676.1971.11879832, 1971.

French, H.M. and Harry, D.G.: Observations on buried glacier ice and massive segregated ice, western Arctic coast, Canada. Permafrost and Periglacial Processes, 1, 1, 31-43. https://doi.org/10.1002/ppp.3430010105, 1990.

Geological Survey of Canada: Surficial geology, western Fosheim Peninsula and eastern Axel Heiberg Island, Nunavut, NTS 49-G and 340-B southwest; Geological Survey of Canada, Canadian Geoscience Map 392 (Surficial Data Model v.2.3.14 conversion of Open File 501), scale 1:125 000. https://doi.org/10.4095/313535, 2022.

Gravenor, C.P., Kupsch, W.O.: Ice-Disintegration Features in Western Canada. J. Geol. 67, 48–64. https://doi.org/10.1086/626557, 1959.

Haines-Young, R.H., Petch., R.J.: Multiple working hypotheses: equifinality and the study of landforms. Trans. Inst. Br. Geogr. 8 (4), 458–466. https://doi.org/10.2307/621962, 1983.

Hallet, B.: Stone circles: Form and soil kinematics. Philosophical Transactions of the Royal Society of London. Series A: Mathematical, Physical, and Engineering Sciences, 371, 2004, 20120357–20120357. https://doi.org/10.1098/rsta.2012.0357, 2013.

Hallet, B., Prestrud, S.: Dynamics of periglacial sorted circles in western Spitsbergen. Quat. Res. 26 (1), 81–99. https://doi.org/10.1016/0033-5894(86)90085-2, 1986.

Ham, N.R., Attig, J.W.: Ice wastage and landscape evolution along the southernmargin of the Laurentide Ice Sheet, north-central Wisconsin. Boreas 25 (3), 171–186, https://doi.org/10.1111/j.1502-3885.1996.tb00846.x, 1996.

Harrison, J.C., Jackson, M.P.A.: Exposed evaporite diapirs and minibasins above a canopy in central Sverdrup Basin, Axel Heiberg Island, Arctic Canada. Basin Res. 26, 567–596. https://doi.org/10.1111/bre.12037, 2014.

Henkemans, E.: Geochemical characterization of groundwaters, surface waters and water-rock interaction in an area of continuous permafrost adjacent to the Greenland ice sheet, Kangerlussuaq, southwest Greenland, 2016.

Hibbard, S. M., Osinski, G. R., Godin, E.: Vermicular Ridge Features on Dundas Harbour, Devon Island, Nunavut. Geomorphology, 395. https://doi.org/10.1016/j.geomorph.2021.107947, 2021.

Holmes, G.W., Hopkins, D.M. and Foster, H.L.: Pingos in central Alaska (p. H1-H40). Washington, DC: US Government Printing Office, 1968.

Hoppe, G.: Hummocky Moraine Regions with special reference to the interior of Norrbotten. Geogr. Ann. 34, 1–72. https://doi.org/10.2307/520144, 1952.

Hyyppä, E., Kukko, A., Kaijaluoto, R., White, J.C., Wulder, M.A., Pyörälä, J., Liang, X., Yu, X., Wang, Y., Kaartinen, H., Virtanen, J.P., Hyyppä, J.: Accurate derivation of stem curve and volume using backpack mobile laser scanning. ISPRS J. Photogramm. Remote Sens. 161, 246–262. https://doi.org/10.1016/j.isprsjprs.2020.01.018, 2020.

Jennings, C.E.: Terrestrial ice streams—a viewfromthe lobe. Geomorphology 75 (1), 100–124. https://doi.org/10.1016/j.geomorph.2005.05.016, 2006.

Johnson, M.D., Clayton, L.: Chapter 10: Supraglacial landsystems in lowland terrain. In: Evans, D.J.A. (Ed.), Glacial Landsystems. London, 228–258, 2003.

Johnson, M.D., Mickelson, D.M., Clayton, L., Attig, J.W.,: Composition and genesis of glacial hummocks, western Wisconsin, USA. Boreas 24 (2), 97–116. https://doi.org/10.1111/j.1502-3885.1995.tb00630.x, 1995.

Jorgenson, M. T., and Y. Shur: Evolution of lakes and basins in northern Alaska and discussion of the thaw lake cycle, J. Geophys. Res., 112, F02S17, https://doi.org/10.1029/2006JF000531, 2007.

Jorgenson, T.M., Shur, Y.L., Walker, H.J.: Evolution of a permafrost dominated landscape on the Colville River Delta, northern Alaska. 7th international conference on permafrost. Yellowknife, Canada: Collection Nordicana, No 55, 1998.

Kääb, A., Girod, L., Berthling, I.: Surface kinematics of periglacial sorted circles using structure-from-motion technology. Cryosphere 8 (3), 1041–1056. https://doi.org/10.5194/tc-8-1041-2014, 2014.

Kessler, M.A., Murray, A.B., Werner, B.T., Hallet, B.: A model for sorted circles as self organized patterns. J. Geophys. Res. Solid Earth 106 (B7), 13287–13306. https://doi.org/10.1029/2001JB000279, 2001.

Knudsen, C.G., Larsen, E., Sejrup, H.P., Stalsberg, K.: Hummocky moraine landscape on Jæren, SW Norway-implications for glacier dynamics during the last deglaciation. Geomorphology 77, 153–168. https://doi.org/10.1016/j.geomorph.2005.12.011, 2006.

Krüger, J., Kjær, K.H. and Schomacker, A.: 7 Dead-Ice Environments: A Landsystems Model for a Debris-Charged, Stagnant Lowland Glacier Margin, Kötlujökull. Developments in Quaternary Sciences, 13, 105–126. https://doi.org/10.1016/S1571-0866(09)01307-4, 2010.

Kukko, A., Kaartinen, H., Hyyppä, J., Chen, Y.: Multiplatform mobile laser scanning: Usability and performance. Sensors (Switzerland). https://doi.org/10.3390/s120911712, 2012.

Kukko, A., Kaijaluoto, R., Kaartinen, H., Lehtola, V. V., Jaakkola, A., Hyyppä, J.: Graph SLAM correction for single scanner MLS forest data under boreal forest canopy. ISPRS J. Photogramm. Remote Sens. 132, 199–209. https://doi.org/10.1016/j.isprsjprs.2017.09.006, 2017.

Kukko, A., Kaartinen, H., Osinski, G. and Hyyppä, J.: Modeling Permafrost Terrain Using Kinematic, Dual-Wavelength Laser Scanning. ISPRS Annals of the Photogrammetry, Remote Sensing and Spatial Information Sciences, 2, 749–756. https://doi.org/10.5194/isprs-annals-V-2-2020-749-2020, 2020.

Lagerbäck, R.: The Veiki moraines in northern Sweden-widespread evidence of an Early Weichselian deglaciation. Boreas, 17, 4, 469–486. https://doi.org/10.1111/j.1502-3885.1988.tb00562.x, 1988.

Liestøl, O.: Pingos, springs, and permafrost in Spitsbergen. Norsk Polarinstitutt Årbok. p. 7-29, 1977.

Liang, X., Wang, Y., Jaakkola, A., Kukko, A., Kaartinen, H., Hyyppä, J., Honkavaara, E., Liu, J.: Forest data collection using terrestrial image-based point clouds from a handheld camera compared to terrestrial and personal laser scanning. IEEE Trans. Geosci. Remote Sens. 53, 5117–5132, 2015.

Lindsay, J.B.: The Whitebox Geospatial Analysis Tools project and open-access GIS. Proceedings of the GIS Research UK 22nd Annual Conference, The University of Glasgow, 16-18 April, https://doi.org/10.13140/RG.2.1.1010.8962, 2014.

Lindsay, J.B.: Whitebox GAT: A case study in geomorphometric analysis. Computers and Geosciences, 95: 75–84. https://doi.org/10.1016/j.cageo.2016.07.003, 2016.

Lundqvist, J.: Rogen (ribbed) moraine—identification and possible origin. Sedimentary Geology, 62, 2–4, 281–292. https://doi.org/10.1016/0037-0738(89)90119-X, 1989.

Mackay, J.R.: The Mackenzie Delta area, N.W. T.; Geographical Branch, Memoir 8, 1963.

Mackay, J.R: The Mackenzie Delta area, Northwest Territories. Geological Survey of Canada Report 23, Energy, Mines and Resources Canada https://doi.org/10.4095/119932., 1974.

Mackay, J.R.: Pingo Growth and collapse, Tuktoyaktuk Peninsula Area,Western Arctic Coast, Canada: a long-term field study. Géog. Phys. Quatern. 52 (3), 271–323. https://doi.org/10.7202/004847ar, 1998.

Mackay, J. R., Burn, C. R.: The first 20 years (1978–1979 to 1998–1999) of active layer development, Illisarvik experimental drained lake site, western Arctic coast, Canada. Canadian Journal of Earth Sciences, 39, 1657–1674, 2002.

Mackay, J.R. and Dallimore, S.R.: Massive ice of the Tuktoyaktuk area, western Arctic coast, Canada. Canadian Journal of Earth Sciences, 29, 6, 1235-1249. https://doi.org/10.1139/e92-099, 1992.

Mckenzie, G.D.: Observations on a Collapsing Kame Terrace In Glacier Bay National Monument, South-Eastern Alaska. J. Glaciol. 8, 413–425. https://doi.org/10.3189/s0022143000027003, 1969.

McKenzie, G.D., Goodwin, R.G.: Development of Collapsed Glacial Topography in the Adams Inlet Area, Alaska, U.S.A. J. Glaciol. 33, 55–59. https://doi.org/10.3189/s0022143000005347, 1987.

Menzies, J., Shilts, W.W.: Subglacial environments. In: Menzies, J. (Ed.), Modern & Past Glacial Environments. Butterworth-Heinemann, pp. 183–278, 2002.

Middleton, M., Heikkonen, J., Nevalainen, P., Hyvönen, E. and Sutinen, R.: Machine learning-based mapping of micro-topographic earthquake-induced paleo-Pulju moraines and liquefaction spreads from a digital elevation model acquired through laser scanning. Geomorphology, 358, 107099. https://doi.org/10.1016/j.geomorph.2020.107099, 2020.

Moore, P. L.: Numerical Simulation of Supraglacial Debris Mobility: Implications for Ablation and Landform Genesis. Front. Earth Sci. 9:710131. https://doi.org/10.3389/feart.2021.710131, 2021.

Möller, P., Dowling, T.P.F.: Equifinality in glacial geomorphology: instability theory examined via ribbed moraine and drumlins in Sweden. GFF 140 (2), 106–135. https://doi.org/10.1080/11035897.2018.1441903, 2018.

Morse, P.D., and Burn, C.R.: Perennial frost blisters of the outer Mackenzie Delta, western Arctic coast, Canada. Earth Surface Processes and Landforms, 39: 200–213. https://doi.org/10.1002/esp.3439, 2014.

Müller, F.: Analysis of some stratigraphic observations and radiocarbon dates from two pingos in the Mackenzie Delta area, NWT. Arctic, 15(4), p.279-288, 1962.

Ó Cofaigh, C., England, J., Zreda, M.: Late Wisconsinan glaciation of southern Eureka Sound: Evidence for extensive Innuitian ice in the Canadian High Arctic during the Last Glacial Maximum. Quat. Sci. Rev. 19, 1319–1341. https://doi.org/10.1016/S0277-3791(99)00104-3, 2000.

Ó Cofaigh, C., Evans, D., and England, J.: Ice marginal terrestrial landsystems: Sub-polar glacier margins of the Canadian and Greenland high arctic. In Glacial Landsystems, ed. D. Evans, Chapter 3, 2003.

Ó Cofaigh, C., Lemman, D.S., Evans, D.J.A. and Bednarski, J.: Glacial landform-sediment assemblages in the Canadian High Arctic and their implications for late Quaternary glaciations. Annals of Glaciology, 28, 195–201. https://doi.org/10.3189/172756499781821760, 1999.

Ommanney, C.S.: A study in glacier inventory: the ice masses of Axel Heiberg Island, Canadian Arctic Archipelago, 1969.

O'Neill, H.B., Wolfe, S.A. and Duchesne, C.: New ground ice maps for Canada using a paleogeographic modelling approach. The Cryosphere, 13(3), p.753-773. https://doi.org/10.5194/tc-13-753-2019, 2019.

Parizek, R.R.: Glacial ice-contact rings and ridges. United States Contributions to Quaternary Research. Geological Society of America Special Paper 123, pp. 49–102, 1969.

Patterson, C. J.: Southern Laurentide ice lobes were created by ice streams: Des Moines Lobe in Minnesota, USA. Sediment. Geol., 111, 1, 249–261. https://doi.org/10.1016/S0037-0738(97)00018-3, 1997.

Patterson, C.J.: Laurentide glacial landscapes: the role of ice streams. Geology 26 (7), 643–646. https://doi.org/10.1130/0091-7613(1998)026<0643:LGLTRO>2.3.CO;2, 1998.

Paul, M.A.: The supraglacial landsystem. In: Eyles, N. (Ed.), Glacial Geology, Oxford, pp. 71–90 https://doi.org/10.1016/B978-0-08-030263-8.50009-9, 1983.

Paulen, R.C., McClenaghan,M.B.: Late wisconsin ice-flow history in the buffalo head hills kimberlite field, north-central alberta. Can. J. Earth Sci. 52 (1), 51–67. https://doi.org/10.1139/cjes-2014-0109, 2014.

Pissart, A.: Palsas, lithalsas and remnants of these periglacial mounds. A progress report. Progress in Physical Geography: Earth and Environment, 26: 605–621. https://doi.org/10.1191/0309133302pp354ra, 2002.

Pissart, A., French, H.M.: Pingo investigations, north-central Banks Island, Canadian Arctic. Can. J. Earth Sci. 13 (7), 937–946. https://doi.org/10.1139/e76-096, 1976.

Pissart, A., French, H.M.: The origin of pingos in regions of thick permafrost, western Canadian Arctic. Quaestiones Geographicae 4, 149–160. http://hdl.handle.net/2268/248067, 1977.

Pollard, W. and Bell, T.: Massive ice formation in the Eureka Sound Lowlands: A landscape model. In Proceedings, Seventh International Permafrost Conference (pp. 903-908). Laval, Quebec City, Quebec, Canada: Université Laval, Centre d'etudes nordiques, Collection Nordicana, 1998.

Pollard, W., Omelon, C., Andersen, D., McKay, C.: Perennial spring occurrence in the Expedition Fiord area of western Axel Heiberg Island, Canadian High Arctic. Can. J. Earth Sci. 36, 105–120. https://doi.org/10.1139/e98-097, 1999.

Porter, C., Morin, P., Howat, I., Noh,M., Bates, B., Peterman, K., Keesey, S., Schlenk, M., Gardiner, J., Tomko, K.,Willis, M., Kelleher, C., Cloutier, M., Husby, E., Foga, S., Nakamura, H., Platson, M., Wethington, M. J., Williamson, C., Bauer, G., Enos, J., Arnold, G., Kramer, W., Becker, P., Doshi, A., D'Souza, C., Cummens, P., Laurier, F., Bojesen, M.: ArcticDEM. https://doi.org/10.7910/DVN/OHHUKH, (Harvard Dataverse, V1), (accessed 23 May 2022), 2018.

Rampton, V. N.: Quaternary Geology of the Tuktoyaktuk Coastlands, Northwest Territories, Memoir 423, Geological Survey of Canada, Ottawa, ON, Canada, 1988.

Ross, N., Brabham, P., Harris, C.: The glacial origins of relict “pingos”, Wales, UK. Ann. Glaciol. 60, 138–150. https://doi.org/10.1017/aog.2019.40, 2019.

Russell, A.J., Roberts, M.J., Fay, H., Marren, P.M., Cassidy, N.J., Tweed, F.S., Harris, T.: Icelandic jökulhlaup impacts: Implications for ice-sheet hydrology, sediment transfer and geomorphology. Geomorphology 75, 33–64. https://doi.org/10.1016/j.geomorph.2005.05.018, 2006.

Samsonov, S.V., Lantz, T.C., Kokelj, S.V. and Zhang, Y.: Growth of a young pingo in the Canadian Arctic observed by RADARSAT-2 interferometric satellite radar. The Cryosphere, 10, 2, 799-810, 2016.

Schmertmann, J.H., Taylor, R.S.: Quantitative data from a patterned ground site over permafrost. U.S. Army Cold Regions Research and Engineering Laboratory Research Report. 96, p. 76, 1965.

Schomacker, A.:. What controls dead-ice melting under different climate conditions? A discussion. Earth-Sci. Rev. 90 (3), 103–113. https://doi.org/10.1016/j.earscirev.2008.08.003, 2008.

Sutinen, R., Hyvönen, E., Middleton, M., Ruskeeniemi, T.: Airborne LiDAR detection of postglacial faults and Pulju moraine in Palojärvi, Finnish Lapland. Glob. Planet. Chang. 115, 24–32. https://doi.org/10.1016/j.gloplacha.2014.01.007, 2014.

Sutinen, R., Hyvönen, E., Middleton, M., Airo, M.L.: Earthquake-induced deformations on ice-stream landforms in Kuusamo, eastern Finnish Lapland. Glob. Planet. Chang. 160, 46–60. https://doi.org/10.1016/j.gloplacha.2017.11.011, 2018.

Sutinen, R., Hyvönen, E., Liwata-Kenttälä, P., Middleton, M., Ojala, A., Ruskeeniemi, T., Sutinen, A., Mattila, J.: Electrical-sedimentary anisotropy of landforms adjacent to postglacial faults in Lapland. Geomorphology 326, 213–224. https://doi.org/10.1016/j.geomorph.2018.01.008, 2019.

Taylor, A.E., Judge, A.S.: Canadian Geothermal Data Collection: Northern Wells. Ottawam, 1976.

Thompson S, Benn DI, Mertes J, Luckman A.: Stagnation and mass loss on a Himalayan debris-covered glacier: Processes, patterns and rates. Journal of Glaciology 62, 233, 467–485. https://doi.org/10.1017/jog.2016.37, 2016.

Thomson, L.I., Osinski, G.R., Ommanney, C.S.L.: Glacier change on Axel Heiberg Island, Nunavut, Canada. J. Glaciol. 57, 1079–1086. https://doi.org/10.3189/002214311798843287, 2011.

Thorsteinsson, R.: Geology, Eureka Sound North, District of Franklin. Geological Survey of Canada, "A" Series Map 1302A, 1 sheet, https://doi.org/10.4095/109125, 1971a.

Thorsteinsson, R.: Geology of Strand Fiord, District of Franklin. Geological Survey of Canada, Map 1301A, scale 1:250 000, 1971b.

Washburn, A.L.: Classification of patterned ground and review of suggested origins. Bull. Geol. Soc. Am. 67 (7), 823–865. https://doi.org/10.1130/0016-7606(1956)67[823:COPGAR]2.0.CO;2, 1956.

Washburn, A.: Periglacial Processes and Environments. Edward Arnold, London, 1973.

Watson, E. and Watson, S.: Remains of pingos in the Cletwr basin, south-west Wales. GeografiskaAnnaler 56A, 213–225, 1974.

Westoby, M.J., Rounce, D.R., Shaw, T.E., Fyffe, C.L., Moore, P.L., Stewart, R.L. and Brock, B.W.: Geomorphological evolution of a debris-covered glacier surface. Earth Surface Processes and Landforms, 45, 14, 3431–3448. https://doi.org/10.1002/esp.4973, 2020.

Wolfe, S.A., Stevens, C.W., Gaanderse, A.J. and Oldenborger, G.A.: Lithalsa distribution, morphology and landscape associations in the Great Slave Lowland, Northwest Territories, Canada. Geomorphology, 204, 302–313. https://doi.org/10.1016/j.geomorph.2013.08.014, 2014.